DESIGN AND DEVELOPMENT OF AN LED-BASED OPTICAL COMMUNICATION SYSTEM

By

Mohammed Al-rubaiai

A THESIS

Submitted to
Michigan State University
in partial fulfillment of the requirements
for the degree of

Electrical Engineering - Master of Science

2015

ABSTRACT

DESIGN AND DEVELOPMENT OF AN LED-BASED OPTICAL COMMUNICATION SYSTEM

By

Mohammed Al-rubaiai

Strong attenuation of most electromagnetic signals in water is the main reason why underwater exploration, surveillance, and other applications currently rely on sub-sea cables and tethers to send data back to the user. While acoustic modems have long been the default wireless communication method for underwater applications, they incur high cost and can only deliver low data rates. In this work, an LED-based optical communication system is presented for applications requiring high data rates, low power, low complexity, and low-to-median communication range.

An LED-based communication system, consisting of a transmitter with a super-bright blue LED and a receiver based on a blue-enhanced photo diode, has been developed and tested with the goal of transmitting data at high rates over distances of at least 20 meters. Test results in a swimming pool show the successful transmission of large data over a distance of 23 meters and at transmission rates of 115200 kbps. This system relies on a line-of-sight connection for communication. Since the change of the relative position and orientation between the transmitter and the receiver will affect the quality of communication link, a mechanism is designed so that the transmitter/receiver modules can be rotated to maintain alignment between the communicating parties, despite the movement of underlying platforms (e.g., robots). A signal strength-based feedback control algorithm is developed to maintain alignment. Experimental results involving a stationary transmitter and a mobile receiver mounted on a terrestrial robot are presented to evaluate the performance of the system.

ACKNOWLEDGMENTS

I would like to express my deepest gratitude to my advisor Professor Xiaobo Tan at Michigan State University for his guidance, caring, and patience, and for providing me with an excellent atmosphere for this thesis work. He consistently steered me in the right direction whenever he thought I needed it. I would like to thank Professors Hassan Khalil and Nelson Sepulveda for serving on my thesis committee. Also, I want to thank John Thon for his help in providing the access to the swimming pool for testing, and Montasser Sharif for helping me in the swimming pool experiments. I would never have been able to finish my thesis without the guidance of Professor Tan, the help from friends, and the support from my family. I would also like to acknowledge the financial support of my research from the Higher Committee for Education Development in Iraq (HCED) and from the US National Science Foundation (IIS 1319602).

Finally, and most importantly, I would like to express my most profound gratitude to my parents for their endless love, consistent support, and encouragement throughout this research.

TABLE OF CONTENTS

LIST OF TABLES

LIST OF FIGURES

Chapter 1

Introduction

More than 70 percent of the Earth's surface is covered by the oceans and contains 97 percent of the planet's water, yet more than 95 percent of the submerged world stays unexplored. The sea and lakes assume an essential part in a number of the Earth's frameworks including atmosphere and climate [15]. It is broadly accepted that the submerged world holds thoughts and assets that will fuel a great part of the up and coming era of science and business. This is confirmed by the considerable investment in supporting the improvement of submerged observatories and underwater robots [16]. One of the most important tasks that these systems and devices need to be able to perform is to communicate with each other and the surface in order to monitor progress or transmit data collected from sensors. The easiest approach to communicate is through a physical connection, for example, a copper cable. In spite of the fact that this takes into consideration effective and rapid communication, a cable results in numerous operational difficulties, constraining the reach and mobility.

Wireless communication is a considerably more feasible answer. Applications of underwater wireless communication range from oil industry to aquaculture, and include pollution instrument monitoring, climate change data recording, study of marine life, and search and survey missions. Underwater wireless sensor networks, for example, are a network of sensors or underwater observatories that collect oceanographic data over an interval of time and send the data to the outside world periodically for processing. Such sensors usually transmit significant amounts of data which require a high-bandwidth link to the outside

world. High bandwidth optical wireless links are one possible solution, especially if coupled to autonomous underwater vehicles (AUVs). Nowadays there are a number of underwater vehicles for a diverse set of applications, such as collecting environmental data, detecting underwater mines, surveying underwater pipelines, and assisting in harbor security. Most AUVs are limited in size, and since they are typically battery-powered, have very constrained power budgets. Optical communications are potentially very power efficient. In addition, the use of high-bandwidth optical sources also has system-level advantages, by reducing the amount of time that an AUV has to stay near a sensor to collect data.

1.1 Traditional Underwater Wireless Communication Methods

1.1.1 Acoustics Communication

Acoustic signals are the most preferred carrier in many applications, owing to their low absorption characteristic for underwater communication. Even though the data transmission is slower compared to other carrier signals, the low-absorption characteristic enables the carrier to travel at longer ranges [17].

Nowadays, commercially available underwater modems are able to transmit up to 30 kbps over distances ranging from a hundred meters to a few kilometers [18]. A few companies are developing acoustics-modems for underwater communication. Table 1.1 lists some examples of commercial acoustic modems. From Table 1.1, it can be seen that in general,when the distance increases, the data rate decreases, while the consumed power increases.

Underwater acoustic communications are generally affected by water temperature, pres-

Table 1.1 Comparison of commercial acoustic modems [1].

Company	Model	Bit Rate (bps)	Distance (km)	Transmitter Power (W)	Receiver Power (W)
EvoLogics	S2CR 48/78	31,200	1	18	1.1
LinkQuest	UWM2000	17,800	1.5	2	0.8
Teledyne Benthos	ATM9XX (PSK)	2,400	6	20	0.7
Desert Star Systems	SAM-1	154	1	32	0.168

sure, salinity of the water, path loss, and variable propagation delay. All these factors determine the temporal and spatial variability of the acoustic channel, and make the available bandwidth of the underwater acoustic channel limited and dramatically dependent on both communication range and frequency, which lead to low bit rates [18].

1.1.2 Electromagnetic Waves

Electromagnetic waves are a form of radiant energy released by electromagnetic processes. Visible light is one type of electromagnetic radiation, and other familiar forms are invisible electromagnetic radiations such as X-rays and radio waves. These waves travel at the speed of light, which is much faster than the sound speed in water.

Electromagnetic waves are highly attenuated in water, which results in short travel distance for the signal because of absorption and scattering. Figure 1.1 shows the attenuation coefficients of different wavelengths. It is clear that attenuation is minimum in the wave length between 400-500 μm. The exact wave length that penetrates the furthest through seawater depends on the characteristics of the specific water, since absorption and scattering are influenced by the chemical and biological makeup of the water, but in general wave lengths in the 470 nm range are attenuated the least [3].

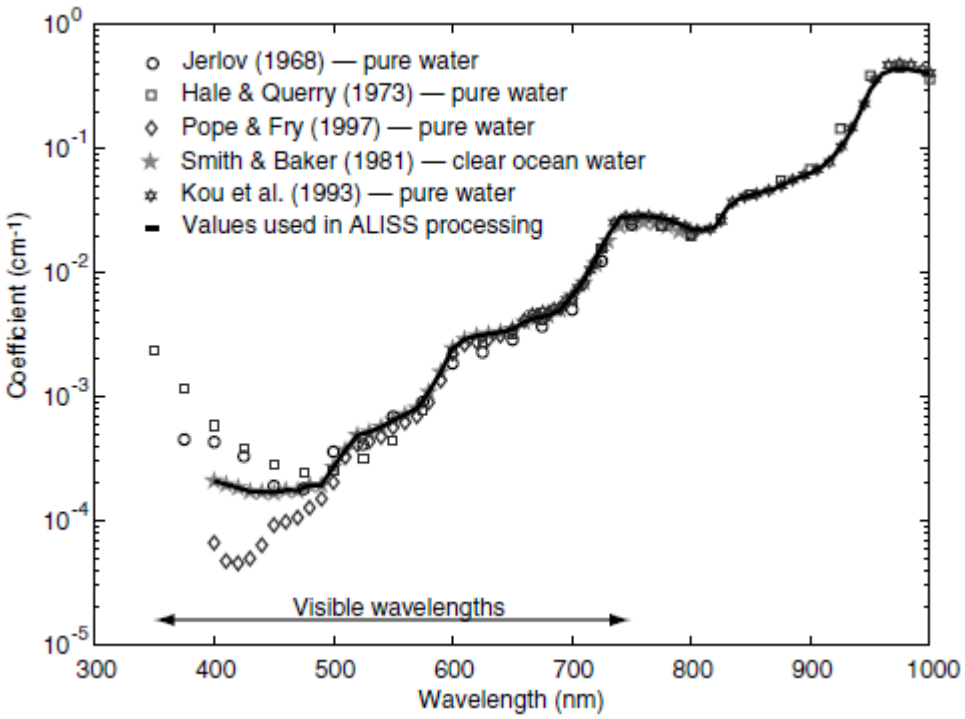

Figure 1.1 Attenuation coefficients of water and seawater [3].

1.2 Underwater Optical Communication

Underwater optical communication systems have grown more popular in recent years with the creation of reliable, low-cost light sources, like light-emitting diodes (LEDs) and lasers. It was in use for communications through air as reported in Smyth et al. [19]. Chen et al. used a 532 nm yttrium aluminum garnet (YAG) laser to generate 10 ns wide, 200 mJ pulses [20]. This corresponded to a 2 MW laser and as a result they could only generate pulses at 50 Hz. They successfully transmited data through a 50 m long water tank. In [21], Cox used a 405 nm laser for transmission and a miniature Hamamatsu R7400U photomultiplier in conjunction with an AD8015 variable gain amplifier (VGA) on the receiving side. His system was tested using a 3.66 m water tank with reliable communication at 500 Kbps. Hanson et al. demonstrated a laser-based system capable of data rates of 1 Gbps over a 2 m path in a tank with 36 dB extinction (absorbents were added to the water) [22]. The performance

of all these systems are impressive, but it is based on a bulky, fragile, and power-inefficient laser setup that is not practical in the context of a small underwater robot. The use of LEDs allows for smaller and cheaper devices, increase eye-safety, and reduces aiming requirements.

Hagem et al. implemented a low-cost and short-range unidirectional optical modem [23]. They use frequency shift keying (FSK) at a data rate of 2.4 Kbps with modulation frequencies of 10 and 12 KHz. Their implementation consisted of a 520 nm, 1.5 mW LED with a 70 degree field of view and an optical detector with a sensitivity of 0.3 A/W. They achieved error-free communication at distances up to 1.1 m underwater without bubbles and up to 0.7 m with bubbles. Lu et al. used an RL5-G13008 Super-Green LED, with a wavelength of 520 nm and a maximum power of 120 mW, and a Silonex SLD-BG2A photodiode together with a band-gap filter to reject infrared wavelengths [24]. The transmitter had a field of view of 90 degrees, and the receiver had a field of view of 120 degrees. They tested their system in a pool at night to avoid ambient light. The system detected 80 percent of the transmitted packets at a communication distance of 10 m. Over 95 percent of the packets were detected at 6 m and below. Brundage implemented a unidirectional communication system using a 465 nm, 4.8 W Titan blue lighting engine (NT-52B1-0469), and a PC10-6B photodiode manufactured by Pacific Silicon Sensor [2]. The light source had a field of view of 22 degree, and the system needed to be aimed. The system achieved error-free communication at 1 Mbps at distances up to 13 m. Schill et al. designed a small optical communication transceiver for a swarm of submersible robots [25]. They used an IrDA physical layer based on the MCP2120 IrDA encoder/decoder chip. Their receiver used a SLD-70 BG2A photodiode together with a MAX3120 for amplification and filtering. They examined three different Luxeon III LEDs for transmission: blue (460 nm, 733 mW), cyan (490 nm, 560 mW), and green (520 nm, 165 mW). They used a byte-oriented UART serial

interface at 57600 bps. They tested their system in air and achieved reliable communication at 1.71 m for 460 nm, 2.02 m for 490 nm, and 1.49 m for 520 nm. All three wavelengths establish a link when tested in a pool at ranges up to 1.7 m. Doniec et al. designed a bidirectional underwater wireless communication system called AquaOptical II [26], which useed 18 Luxeon Rebel LEDs and an avalanche photodiode (APD). The LEDs transmitted at a wavelength of 470 nm with up to 1.126 W of radiant flux each, resulting in a total transmit power of 20 W. The system also utilized an avalanche photo-diode because of its increased dynamic range and quantum efficiency. It operates over distances of 50 m at a data rate of 4 Mbps.

Anguita et al. implemented a transmitter that used 12 LEDs arranged on a circle to transmit omnidirectionally in the plane [27], [28]. In two different implementations they used different LEDs. The first was a Ledman LL1503PLBL1-301 with optical power 15 mW and a 30-degree field of view. The second is an Evergreen Electronic DLE-038-045 with optical power 20 mW and a 30 degree field of view. They proposed an 18 LED omnidirectional transmitter design in the shape of an octahedron. Their receiver consisted of a Hamamatsu S5971 APD with an area of 1 mm^2 and a sensitivity of 0.2 A/W at 470 nm. The output signal was fed through a 10 KHz to 20 MHz bandpass filter, an amplifier with automatic gain control (AGC) based on LT1006, and a comparator to digitize the incoming signal using thresholding. They tested their system with a square wave at distances of up to 2 m and reported the voltage swing after the AGC. They showed that their AGC allowed for pulse detection from distances of a few cm to 10 m in air.

In Table 1.2 a comparison of state-of-the-art underwater optical communication systems is presented. The information provided in different papers was not standardized. Therefore, we compare these systems on the main device elements (light source and light detector),

range of communication, data rate, and whether they require line-of-sight. From Table 1.2, it can be seen that the data rate speed is higher when avalanche photodiodes or photomultipliers instead of photodiodes are used, which is accompanied with higher cost and power consumption. A similar observation applies to the light source; for example, a longer communication range typically requires higher power consumption.

Table 1.2 Comparison of underwater optical communication systems.

	Light source	Light detector	Range (m)	Baud rate (bps)	Line of sight
Hanson et al. [22]	Laser diode	Avalanche photodiode	2	1 G	Required
Cox [21]	Laser	Photomultiplier	3.66	500 K	Required
Brundage [2]	High-power LED	Photodiode	13	1 M	Required
Doniec et al. [26]	18 High-power LEDs	Avalanche photodiode	50	4 M	Required
Anguita et al. [27]	12 LEDs arranged on a circle	Avalanche photodiode	2	100 K	Not required
Rust et al. [29]	High-power LED	8 Photodiodes	23	112.5 K	Not required

1.2.1 Overview of Contributions

The contributions of this research r include the development and characterization of a low-power, cost-effective, high data-rate optical communication system with active alignment maintenance. The alignment maintenance capability greatly alleviates the requirement of line-of-sight for communication and facilitates the use of the developed system for mobile robots. A more detailed account of the contributions follows.

First, on the hardware side, we describe the design, development, and characterization of an optical communication system, which allows for relatively high data rate (115200 Kbps) underwater communication over 23 meters.

Second, we present a signal strength model for the developed optical communication system. Such a model will be helpful in developing the estimation and control algorithms in alignment maintenance as well as in guiding the optimal design of the system.

Finally, we present an active control algorithm for maintaining the alignment of the receiver with the transmitter for LED-based communication systems. The algorithm uses the received signal strength as feedback for adjusting the receiver angles. We demonstrate the effectiveness of this algorithm via experiments involving a mobile robot.

Chapter 2

System Design, Implementation, and Characterization

The underwater optical communication system mainly consists of two parts, the transmitter and the receiver. The transmitter converts the electrical signal into an optical signal. That signal passes through the medium and is picked up by the receiver. The receiver detects the optical signal, and converts it back into an electrical signal for data processing. There are a variety of light sources and detectors to consider for this system. Lasers and photomultiplier tubes offer high performance, and are expected to be used in many underwater optical communication systems. However, these components are relatively expensive and can have large form factors. An alternative solution would be to use the much cheaper LEDs as transmitters and photodiodes as receivers. In addition to the transmitter and the receiver, the system also includes a mechanism for rotating the transmitter/receiver, to maintain communication despite the movement underlying platform (for example, a robot). In this chapter we discuss the details on the hardware design, and present some characterization results on the system's underwater communication performance.

2.1 Design Constraints

The main motivation for this thesis is that it could provide a feasible high-speed communication between underwater robots that collaboratively perform a specific task. In order to do that, we will need to consider some design constrains. In particular, the system needs to have small footprint and consume low power for integration into underwater robots. It also needs to work without perfect alignment between the transmitter and the receiver, since it will be difficult for a robot to hold the position and the orientation, because of both the nature of the underwater environment and the mobility nature of a robot. It is also preferable that the system will require little to no maintenance for long periods of time. Finally, it is desired to have relatively long communication range and relatively high data rate.

2.2 Transmitter

The role of the optical transmitter is to convert the electrical signal into light pulses, and launch the resulting optical signal into the transmission channel. It consists of the input signal, the optical driver system, the light source, and light-beam conditioning optics, such as reflectors and lenses.

2.2.1 Light Source

The first step when designing the transmitter is to decide which light source to use, since the rest of the transmitter is designed to support the chosen source. Theoretically speaking, any light source could be used, from an incandescent lamp to a laser, but the size, power and switching speed constraints placed on the system narrow down the selections to two feasible choices: light emitting diodes (LEDs) and laser diodes (LDs).

An LED, examples of which are shown in Figure 2.1, is a semiconductor device that emits visible light when an electric current passes through it. The light is not particularly bright, but in most LEDs it is monochromatic, occurring at a single wavelength. The output from an LED can range from red (at a wavelength of approximately 700 nm) to blue-violet (about 400 nm). Some LEDs emit infrared (IR) (830 nm or longer); such a device is known as an infrared-emitting diode (IRED) [30]. An LED consists of two elements of processed material, called P-type semiconductor and N-type semiconductor. These two elements are placed in direct contact, forming a region called the P-N junction. In this respect, the LED resembles most other types of diodes, but there are important differences. An LED has a transparent package, allowing visible or IR energy to pass through [31].

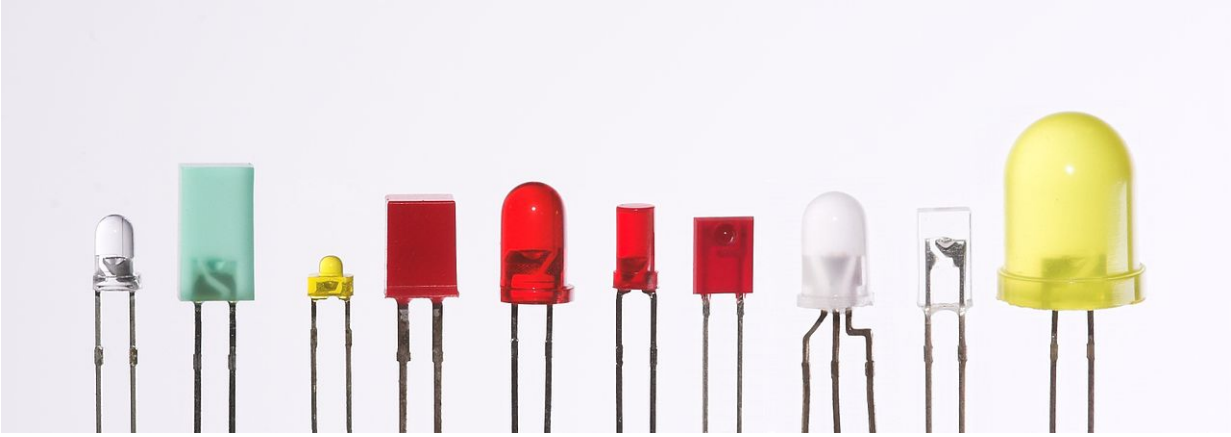

Figure 2.1 Common example of LEDs [4].

Benefits of LEDs include:low power requirement since most types can operated with battery power supplies, and good efficiency since most of the power supplied to an LED is converted into radiation in the desired form, with minimal heat loss. When properly installed, an LED can function for decades. Because of their simplicity and reliability, LEDs are relatively cheap and widely available [30].

Laser diodes (LDs) are a later innovation which has evolved from fundamental LED

manufacturing methods [32]. LDs (see Figure 2.2 for an example) still rely on the transition of carriers over the band gap to create radiant photons; however, alterations to the device structure permit such devices to effectively deliver coherent light over a narrow optical bandwidth [30]. Laser diodes form a subset of the larger classification of semiconductor p-n junction diodes. Forward electrical bias across the laser diode causes the two species of charge carrier, holes and electrons, to be injected from opposite sides of the p-n junction into the depletion region. Holes are injected from the p-doped region, and electrons from the n-doped region. Due to the use of charge injection in powering most diode lasers, this class of lasers is sometimes termed "injection lasers" or "injection laser diode" (ILD).

Figure 2.2 An example of Laser Diode [5].

As diode lasers are semiconductor devices, they may also be classified as semiconductor lasers. Either designation distinguishes diode lasers from solid-state lasers [33]. Stimulated emission only happens after a threshold current has been reached. It has a very small recombination time constant, which means that laser diodes have a much faster rise time, allowing for modulation bandwidths in the GHz range and high optical power emissions in a very narrow optical spectrum width, around 1 nm [30]. Unfortunately, stimulated emission is challenging to maintain. Laser diodes are very sensitive to changes in temperature and current - the wavelength of the laser diode can change by about 0.1 nm/° [34] and the efficiency and threshold current can change significantly due to aging and temperature [20].

Thermal, optical and electrical feedback is necessary to sustain operation and prevent the laser diode from failing. This adds complexity and cost to the system. The sensitivity of laser diodes results in shorter life times and lower reliability. Table 2.1 presents a comparison of the features of LDs and LEDs for wireless optical applications based on [30], [32].

Table 2.1 LED vs. laser diode for wireless optical communication.

Characteristics	LED	Laser Diode
Optical spectral width	25-100 nm	0.1 to 5 nm
Modulation bandwidth	Tens of kHz to hundereds of MHz	Tens of kHz to tens of GHz
Special circuit required	None	Threshold and temperature compensation circuitry
Eye safety	Considered eye-safe	Must be rendered eye-safe
Reliability	High	Moderate
Cost	Low	Moderate to high

From previous discussions it is clear that both LEDs and laser diodes have strengths and weaknesses when it comes to wireless optical communications. Laser diodes can switch faster and have higher optical power output, but LED systems are cheaper, simpler, and more reliable. While the coherence and minimal divergence of laser diodes are optimal for fiber optic communication systems, they do not play as big a role in wireless optical communication. Additionally, although laser diodes can switch faster, LEDs can switch fast enough for many applications. Since the goal is to have a small, cheap, reliable communication system, LEDs are selected as the light source for the optical transmitter in this work.

2.2.2 LED Selection

In order to choose the right LED, we need to check the commercially available high brightness blue LEDs. Since we need to achieve relatively long range of communication (over 20 m) with low power consumption, the maximum amount of optical power in the 470 nm range is needed. This can be achieved by choosing super-bright LEDs or by using multiple LEDs. Different LED manufacturers were researched to find the brightest blue LED on the market. Table 2.2 shows a comparison of various high-power LEDs on the market (all data taken from their respective data sheets). It is clear that high-power LEDs can give off a luminous flux of 30-60 lumens. This is compared to the less than 1 lumen that standard LEDs produce. While other colored LEDs, such as Amber, have been around for a long time and are able to produce upwards of 130 lumens per LED, blue LED technology is not as advanced and therefore has a lower lumen output.

Table 2.2 Comparison of commercially available high brightness blue LEDs [2].

Manufacturer	Model	Wave Length (nm)	Luminous Flux (lm)
Atlas	NT-42C1-0484	460-470	63
AOP	PU-5WAS	455-475	54
Lumileds	LXML-PBO1-0023	460-490	48
Kingbright	AAD1-9090QB11ZC/3	460	35.7
Ligitek	LGLB-313E	460-475	30.6
Toshiba	TL12B01(T30)	460	6
Lumex	SML-LX1610USBC	470	5
Cree	XREBLU-L1	465-485	30.6
Typical(not high-power)	LED	470	<1

The electric power requirement for super-bright LEDs is generally 1-5 Watts and draws 700-1000 mA current, which means that they require a forward voltage of 2-5 volts. In

order to maximize light output, more LEDs are desirable, but this must be balanced with the system power limitations. Usually, an underwater robot that will be equipped with the transmitter will carry a 12 - 24 volt battery, so it makes sense to limit the number of LEDs. Additionally, as more LEDs are added, optical and thermal properties must be taken into account. Some of the electricity in an LED is converts to heat rather than light. If this heat is not removed, the LEDs run at higher temperatures, which not only lowers their efficiency, but also makes the LEDs less reliable. Therefore, thermal management of high power LEDs is very important. It is necessary to keep the junction temperature below 120 °C to run the LED's for maximum lifetime [35]. Even though LEDs are not as sensitive to high temperatures as laser diodes and do not require thermal monitoring, high-power LEDs must still be fully thermally coupled to heat sinks, which are passive heat exchangers that cool a device by dissipating heat into the surrounding medium.

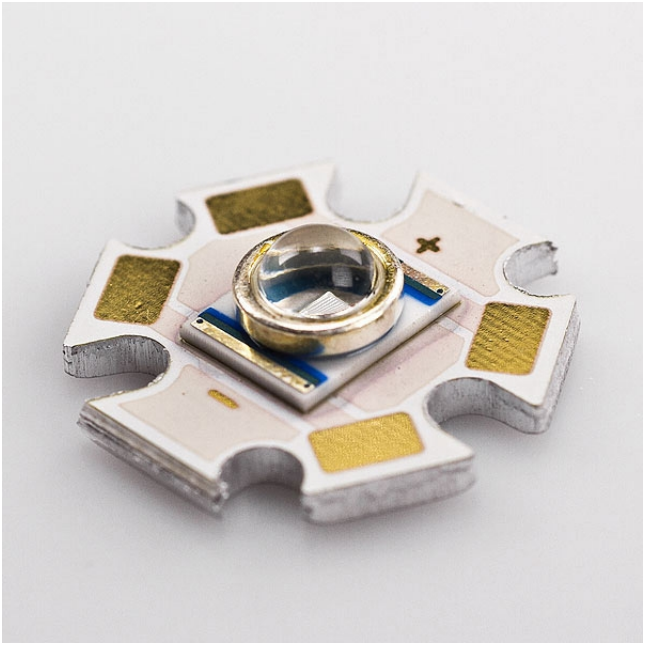

Figure 2.3 Cree XR-E LED attached to a heat sink [6].

For simplicity of the system and to ensure proper operation, it is decided to look for

an off-the-shelf LED. Designing specialized optics and heat sinks is not in the scope of this study. Although many LED manufacturers make single LED chips, very few integrate them with heat sinks and lenses. One of these companies, Super Bright LEDs, does just that, and has very good bright blue LEDs for the purpose of this project. They use Cree XR-E Series LED blue Lighting System (see Figure 2.3) from Cree Company, which provides 30.6 lumens at 1 A and require 3.3 volts [7]. It comes assembled with a heat sink.

2.2.3 LED Driver

In order to modulate the LED (turn it on and off) in correlation with binary data, a circuit must be designed to power it. The circuit needs to provide sufficient current to light the LED at the required intensity, but must limit the current to prevent damaging the LED. LEDs are current-controlled devices (Figure 2.4), which means that the intensity of the output light is linearly related to the supply current. And since the voltage drop across an LED is approximately constant over a wide range of operating current, a small increase in applied voltage greatly increases the current (Figure 2.5) [7].

Commercially available constant-current LED drivers are available. One example is the BuckPuck LED Power Modules, which is a current-regulated driver for powering LEDs. It is used for powering all types of high-brightness and high-power LED packages and LED arrays. It also exhibits high efficiency and requires no external current-limiting resistors or additional heat sinking for operation. It can dim connected LEDs using the internal 5 VDC voltage reference by varying the control voltage [36]. Unfortunately, it is designed for lower speed switching applications, such as LED dimming, and therefore, it is not optimized for the high-speeds optical communication requirements in this project. Another way of controlling LEDs is to provide a constant voltage and limit the current passing through the

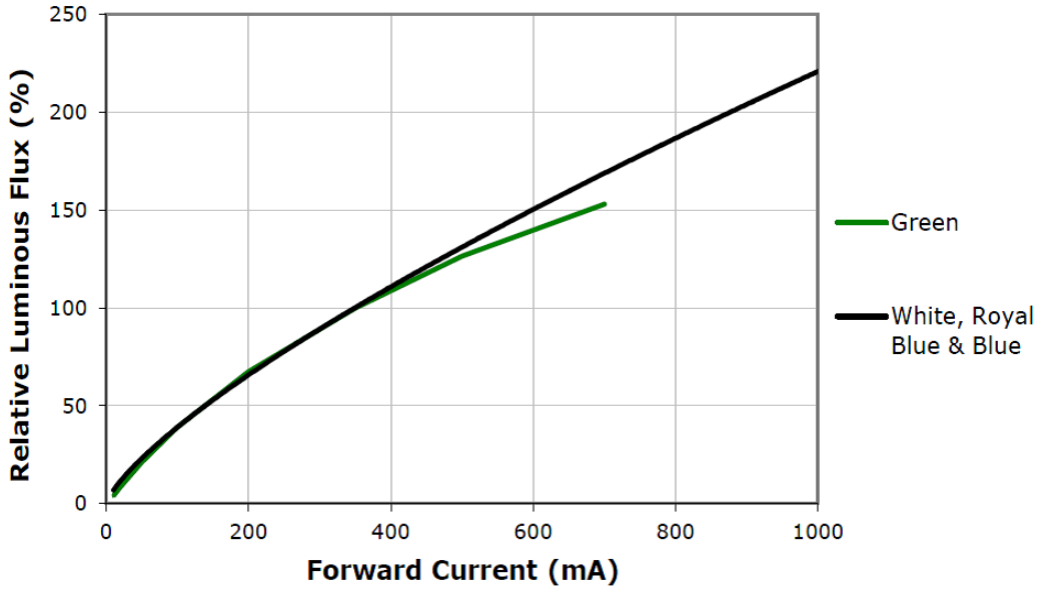

Figure 2.4 Relative flux vs. current relation for Cree XR-E LED (black curve for blue light LED) [7]

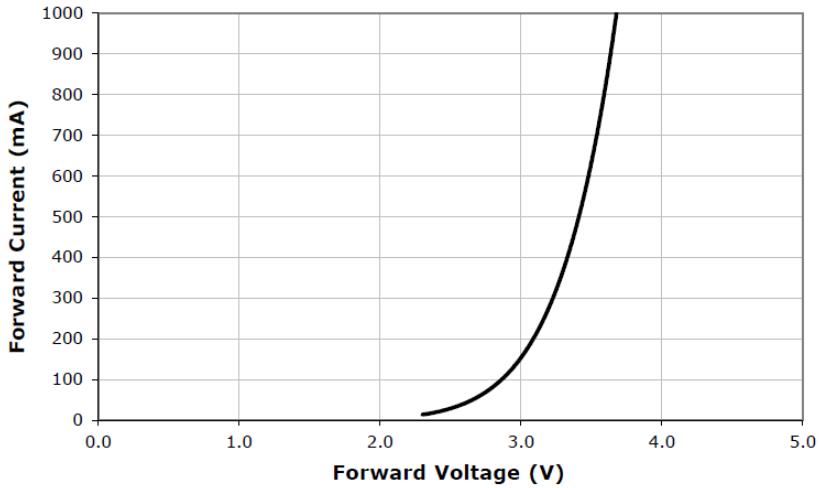

Figure 2.5 Electrical Characteristics for Cree XR-E LED [7].

LEDs using resistors. In this situation, an electronically controlled switch like a transistor can be used to start and stop the flow of current through the LEDs, turning them on and off. A MOSFET (metal oxide semiconductor field-effect transistor) is used in the LED driver circuit. MOSFETs are a type of transistors used for amplifying or switching electronic signals. A MOSFET consists of a drain, a gate, and a source. When there is no voltage difference between the gate and the source, there is a very high resistance between the drain and the source so minimal current flows from the drain to the source - the MOSFET is 'off'. If, however, the gate is supplied with a voltage, the drain-source channel becomes less resistive and the MOSFET is 'on' [37]. Once the gate threshold voltage has been reached, the MOSFET is fully on and the only resistance between the drain and the source is the drain-to-source-on resistance.

The MOSFET is by far the most common transistor in both digital and analog circuits, although the bipolar junction transistor was at one time much more common. The main advantage of a MOSFET transistor over a regular transistor is that it requires very little current to be turned on (less than 1 mA), while delivering a much higher current to a load (10 to 50 A or more). However, the MOSFET requires a higher gate voltage (3-4 V) to be turned on. MOSFETs are better suited for this application compared to bipolar transistors because they have a much lower drain-to-source-on resistance [37]. This means that they will produce a smaller voltage drop and can handle larger currents. Additionally, MOSFETs are better than junction field-effect transistors (JFETs) because they have much larger gate-input impedance. This means that they draw very little gate current. This is advantageous since the computer or the integrated circuit (IC) sending the data signal to the MOSFET typically cannot source a lot of current. If the gate impedance were lower, more current would be needed to change the gate voltage. Even though the gate impedance is high, there

is also a gate capacitance. The larger the gate capacitance, the more current that is needed to charge the gate before the voltage will change.

MOSFETs are available in two basic forms: N channel and P channel (Figure 2.6). For an N channel MOSFET, the source is connected to ground. We can easily raise the voltage on the gate, to enable the current to flow. If no current is to flow, the gate pin should be grounded. For a P channel MOSFET, the source is connected to the power rail. In order to allow the current to flow, the gate needs to be pulled to ground. To stop the current flow, the gate needs to be pulled to power rail [37].

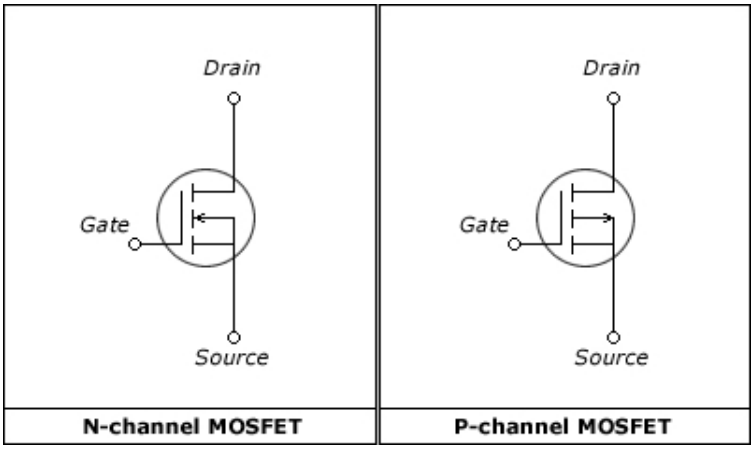

Figure 2.6 MOSFET Schematic Symbols [8].

There are different types of LED driving circuits. In this design a totem pole configuration circuit is adopted. Such a configuration is mainly used to amplify square waves into stronger square waves for driving other types of semiconductors faster. A totem pole consists of a P channel and an N channel MOSFET arranged drain to drain, with their gates coupled together. The output signal is taken from the point where the two drains meet.

There are many commercially available MOSFETs in a push-pull configuration. For this application, a MOSFET that could quickly switch more than 5 V at 2 A is needed. This means that it has to have a drain-to-source breakdown voltage of at least 10 V and

a minimal rise and fall time. Additionally, it has to be able to operate from TTL logic levels, which means that the gate threshold voltage has to be below 5 V. After comparing various MOSFETs, we select IRF7307PbF. With a drain-to-source breakdown voltage of 20 V and a maximum drain current of 5 A, it can adequately handle the power requirements of the LEDs. Additionally, it has a very short rise time of 42 ns [38]. Figure 2.7 shows the transmitter circuit schematic.

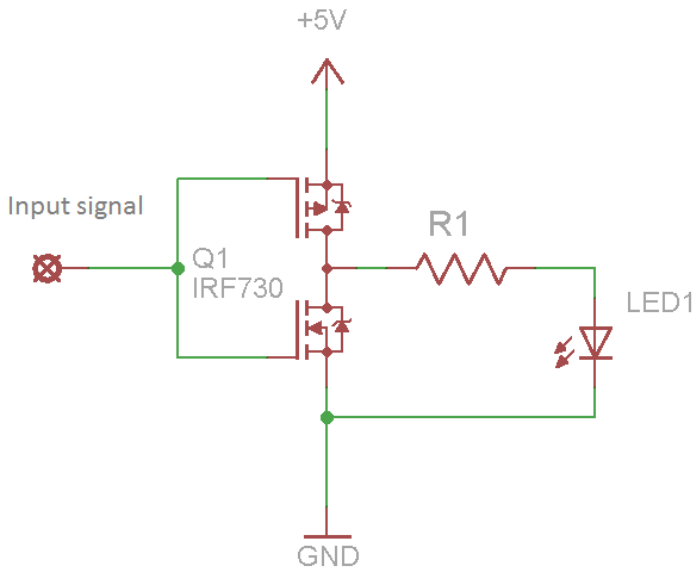

Figure 2.7 Transmitter circuit schematic.

The TTL data signal (0-5 V) goes into the gates of the two MOSFETs, which when on, allow the current to flow through the LEDs and current-limiting resistors, which are powered by the 5 V power rail. A resistor of 2 Ω limits the current that flows through the LEDs to 1 A.

2.3 Receiver

The detector is a device that converts the optical signal received from the transmitter into an electrical signal. Like the transmitter, the detector of the receiver will determines the design of the rest of the system, which will condition the detector output into a usable electrical form. Accordingly, the detector must be selected before the rest of the receiver elements.

2.3.1 Light Detector

Light sensing applications vary widely from specialized scientific instrumentation that needs to detect individual light-photons to systems that control high-speed welding and cutting lasers that produce kilowatts of optical power. Fortunately, there are sensors for almost any application imaginable:from a photomultiplier tube which gives a large voltage pulse for every photon it detects [37], to cooled thermo-piles that absorb kilowatts of power providing a thermocouple voltage proportional to the optical power absorbed [30]. In our application, a detector needs to quickly respond to all incident photons sent by the transmitter without introducing additional noise. Additionally, it needs to be small, robust, cheap, and power-efficient. There are many types of photodetectors which may be appropriate in a particular case.

The first one is the photoresistor (see Figure 2.8 for an example), also known as light-dependent resistors (LDR). An LDR is a type of photoconductor, meaning that its conductivity changes when exposed to electromagnetic radiation such as visible light [37]. An LDR is usually used to indicate the presence or absence of light, or to measure the light intensity. In the dark, its resistance is very high, sometimes up to 1 M ohms, but when the LDR sensor is exposed to light, the resistance drops dramatically, even down to a few ohms, depending

on the light intensity. LDRs have a sensitivity that varies with the wavelength of the light applied and are nonlinear devices. Due to their slow response [30], usually it takes time in milliseconds for a photo-resistor to fully respond to the presence of light, which makes it not feasible for high-speed optical communication.

Figure 2.8 An example of photoresistor [9].

Another type of photodetector is the phototransistor (see an example in Figure 2.9), which is a device that converts light energy into electric energy. They produce both current and voltage. This is because a phototransistor is made of a bipolar semiconductor and focuses the energy that is passed through it. Phototransistors are generally encased in a clear container in order to enhance light as it travels through [39]. A phototransistor generally has an exposed base that amplifies the light that it comes in contact with. This causes a relatively high current to pass through the phototransistor. As the current spreads from the base to the emitter, the current is concentrated and converted into a voltage [30]. Phototransistors are moderately fast and are relatively robust with regard to noise.

Photodiodes are widely used detectors for high-speed applications. See Figure 2.10 for an example. There are different types of photodiodes and they work in slightly different ways, but the basic operations remain the same for all of them [39]. PIN photodiode is a

Figure 2.9 An example of a phototransistor [10].

photodiode with an intrinsic (undoped) region in between the n- and p-doped regions, and it is a semiconductor device that converts light into current. The current is generated when photons are absorbed in the photodiode. When a photon of sufficient energy strikes the diode, it creates an electron-hole pair. This mechanism is also known as the inner photoelectric effect. If the absorption occurs in the junction's depletion region (an insulating region within a conductive region), or one diffusion length away from it, these carriers are swept from the junction by the built-in electric field of the depletion region. Thus holes move toward the anode, and electrons toward the cathode, and a photocurrent is produced. The total current through the photodiode is the sum of the dark current (current that exists in the absence of light) and the photocurrent, so the dark current must be minimized to maximize the sensitivity of the device [14].

PIN photodiodes do not have any internal gain, since each photon can only excite one electron at most, but the photocurrent is linearly proportional to the illuminance. Additionally, since photons can go through a diode without exciting any electrons, photodiodes do not have the sensitivity (quantum efficiency) of photomultiplier tubes, which can detect single photons. Photodiodes can have a response time in nanoseconds and are relatively robust to noise [30]. They are small, robust, and affordable.

Figure 2.10 An example of a photodiode [11].

An avalanche photodiode (APD) is a highly sensitive semiconductor device that uses the photoelectric effect to convert light to electricity. See Figure 2.11 for an example. It is similar to PIN photodiodes, except that they can generate multiple electron-hole pairs as a result of absorbing a single photon by the avalanche process through applying a high reverse bias voltage (typically 100-200 V in silicon) [14]. As a result, the avalanche photodiode is far more sensitive. However, it is found that it is not nearly as linear, and additionally the avalanche process means that the resultant signal is far noisier than one from a PIN diode [37].

Figure 2.11 An example of an avalanch photodiode [12].

The most sensitive light detector is the photomultiplier (see Figure 2.12 for an example), which is optically connected to the sodium iodide crystal. Its purpose is to convert the light energy from the crystal to electrical energy and amplify the resultant pulse of electricity. Photomultipliers are typically constructed with an evacuated glass housing, containing a photocathode, several dynodes, and an anode. Incident photons strike the photocathode material, which is usually a thin vapor-deposited conducting layer on the inside of the entry window of the device [30]. They can have a response time of less than a nanosecond but they are also expensive and fragile, come in big size, and consume large amount of power [14], which makes them a bad choice for application of underwater optical communication.

Figure 2.12 An example of a photomultiplier [13].

2.3.2 Optical Sensor Selection

Each optical sensor has advantages and disadvantages as described in the previous subsections, and the selection process will depend on many factors (Table 2.3). For our application, a sensor that is fast, small, cheap and low-power is required, therefor it is clear that pho-

todiodes fit the requirements necessary for wireless underwater optical communications. A PIN photodiode is chosen over the avalanche photodiode because of the high bias voltage required to operate avalanche photodiodes, as well as their sensitivity to noise and their higher complexity of control circuitry.

Table 2.3 Comparison of light detectors [19], [24], [26].

	Size	Response Time	Photocurrent Gain	Linearity	Cost
Photoresistor	Small	Slow <1 Hz	Little	Over small region	Cheap
PIN photodiode	Small	Fast Tens of MHz to tens of GHz	Unity	Exellent	Cheap
Avalanche photodiode	Small	Fast Hundreds of MHz to tens of GHz	100-100000	Not Linear	Expensive
Phototransistor	Small	Moderate <250 KHz	100-1500	Good	Cheap
Photomultiplyer	Large	Fastest >1GHz	>1Million	Good	Expensive

Since a blue light LED is used, it makes sense to choose a photodiode that is more sensitive to blue light. Unfortunately most photodiodes are sensitive to the red or infrared spectrum. But there are a series of photodiodes called blue-enhanced, which have significant sensitivity to blue light. There are many manufacturers of photodiodes, but few produce blue-enhanced photodiodes. Advanced Photonix offers photodiodes with high quantum efficiency at 410 nm, low dark current, and fast rise time. The product with part number PDB-V107 (Figure 2.13) is selected. It has a relatively large active area (20.6 mm^2). A bigger active area means more sensitivity and shorter rise time (20 ns), and thus higher bandwidth. A 12 V reverse

bias across the photodiode is used to increase the bandwidth and quantum efficiency [14].

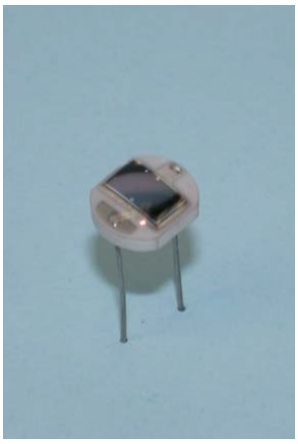

Figure 2.13 Picture of blue-enhanced photodetector (PDBV107) [14].

2.3.3 Receiver Circuit Design

After the photodiode has been selected as a light detector, the design of the required electronic circuitry to process the photodiodes current signal is next. A main component needed is a transimpedance amplifier to convert the photodiode current signal into a voltage signal, which then goes through a filter to reduce the noise. After that it will be amplified and finally made compatible with TTL voltage levels.

Transimpedance amplifiers (TIAs) are used to convert the current output of sensors like a photodiode to voltage signals, because many circuits and instruments can only accept a voltage input. An operational amplifier with a feedback resistor from the output to the inverting input is the most straightforward implementation of such a TIA. However, even this simple TIA circuit requires careful trade-offs among noise gain, offset voltage, bandwidth, and stability. Clearly stability in a TIA is essential for good, reliable performance.

Figure 2.14 shows the schematic of a transimpedance amplifier. The value of the resistor, R_f, determines the gain of the transimpedance amplifier. The feedback capacitor, C_f, is

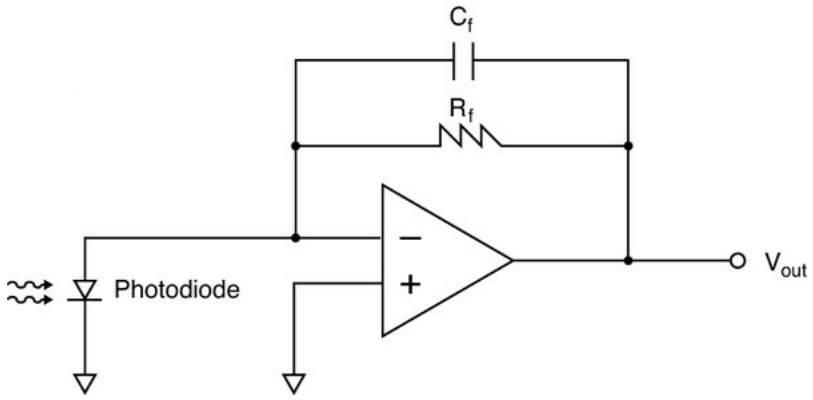

Figure 2.14 Schematic of a transimpedance amplifier for amplifying the photodiode output.

used to stabilize the circuit and reduce overshoot. Although there are equations to help determine the ideal value of C_f, the precise value will need to be tuned experimentally to account for the specifics of each layout.

For this application, high speed and high gain of the TIA are important. Texas Instruments' THS4631 op-amp is chosen because it has a very high gain bandwidth product of 210 MHz and can run off the +12/-12 Voltage rails [40]. It is wired without the feedback capacitor initially. If the feedback resistor is too low, the gain is very small and the system can have too much ringing and noise, whereas if the feedback resistor is chosen to be too large, the gain is too high, saturating the signal and reducing the bandwidth. For these reasons a feedback resistor value of 100 KΩ chosen as a good compromise between high gain and high bandwidth. After the feedback resistor has been determined, testing is done to determine the best C_f for the circuit. If C_f is chosen to be too large, the time constant of the circuit will be too long and the switching speed will be low. When the circuit is built on a printed circuit board (PCB), the feedback capacitor value is chosen, since there is less stray capacitance in the PCB.

After the TIA stage, the signal goes through an electronic filter. The filter is an analog circuit that performs signal processing functions, for an example, removing unwanted

frequencies from the signal, enhancing wanted ones, or both. In this application an active analog low-pass filter is used to remove the unwanted noise. The Linear Technology LTC1560-1 IC is used. Its 5th-order, continuous-time, low-pass elliptic filter operates with 5V power supply, has a power-saving mode, does not require any external components, and is available in an SO-8 surface mount package.

After the signal is processed with the low-pass filter, an inverting voltage amplifier is used to convert the signal from a negative voltage to a positive voltage and amplify it so that even very small signals, received when the transmitter is far away from the receiver, can be detected.

By the same way that we select the transimpedance amplifier component, the voltage amplifier must be an op-amp that is capable of high gains at high speeds. The response time of the op-amp must also be taken into account. The choice is to use an Analog Devices op-42 IC. It is a high-speed, fast-settling (1 ms response time), precision operation amplifier, and it comes in an SO-8 surface mount package.

The final stage in the receiver circuit is to convert the data signal into TTL compatible levels (0 and 5 Volt). Since the previous step is an amplifier running off a ± 10 Volt power rail, the signal coming from the amplifier can be anything between 0 and +10 Volts, depending on the amplitude of the signal going into the amplifier from the TIA. A comparator takes two signals, compares them, and outputs a digital signal indicating which is larger. If the input signal is larger than the reference signal, the comparator output goes high, and vice versa. The high and low output voltages of the comparator are set by the circuit design, and in this case, a 'high' output of +5 Volts and a 'low' output of 0 Volts are desired.

An op-amp is used as a comparator. The reference voltage is connected to the inverting input and the signal is connected to non-inverting input. The product AD790 is selected as

the comparator because it has a short delay time (45 ns), can operate off the already existing +12 Voltage rail, and can handle input signals up to +12 Volts. A potentiometer is used to create a voltage divider to supply the reference voltage. This allows the reference voltage to be easily tuned during testing. A lower reference voltage means that any small signal could trigger the comparator, possibly making the circuit react to noise, but also allowing it to respond to very low input signals.

Once the tests have been conducted, a finalized circuit layout is determined. Figure 2.15 shows the schematic of the receiver circuit. The printed circuit boards (PCBs) and the boards assembled with components for the transmitter and the receiver are shown in Figures 2.16 and 2.17, respectively. The transmitter and the receiver circuits are divided into three and four modules, respectively. For the transmitter, the first modules holds the LED and the high-power resistor, the second module contains the LED driver circuit, and the third module holds the voltage regulator. For the receiver, the first module contains the transimpedance amplifier circuit with the photodiode, the second one is the low pass filter , the third is the amplification stage for the filtered signal, and the last module is the comparator circuit.

Each module is one inch in diameter to make the device footprint as small as possible. These modules are connected withe each other by using header pins, which will serve as electrical and mechanical connections. This configuration will also allow us to change parts of the circuits for maintenance or upgrade. The fully assembled transmitter and receiver are shown in Figure 2.18.

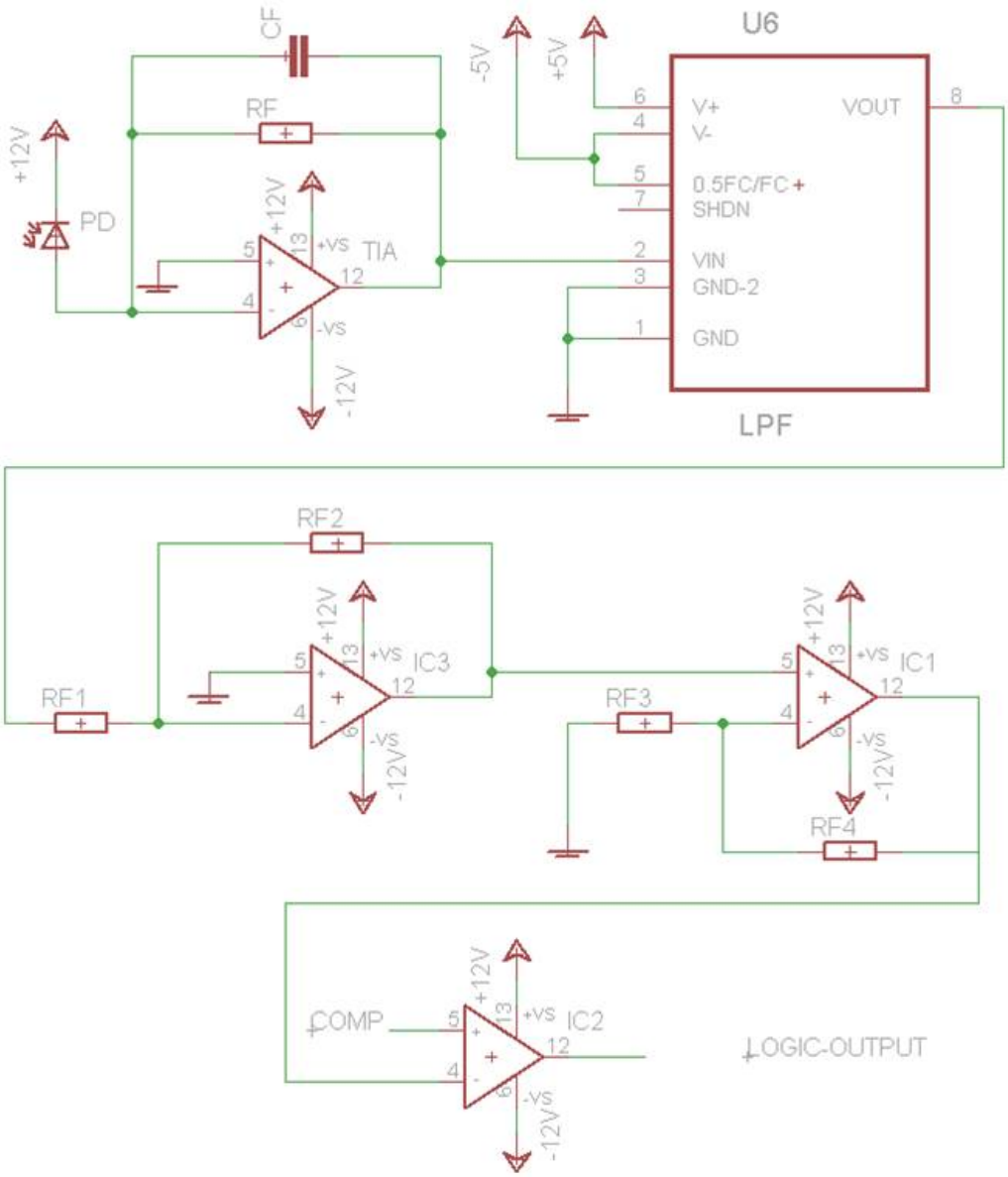

Figure 2.15 Schematic of the receiver circuit. The values of the final circuit components are:RF = 100 KΩ, CF = 0.5 pF, RF1 = RF2 = RF3 = 1 KΩ, and RF4 = 10 KΩ.

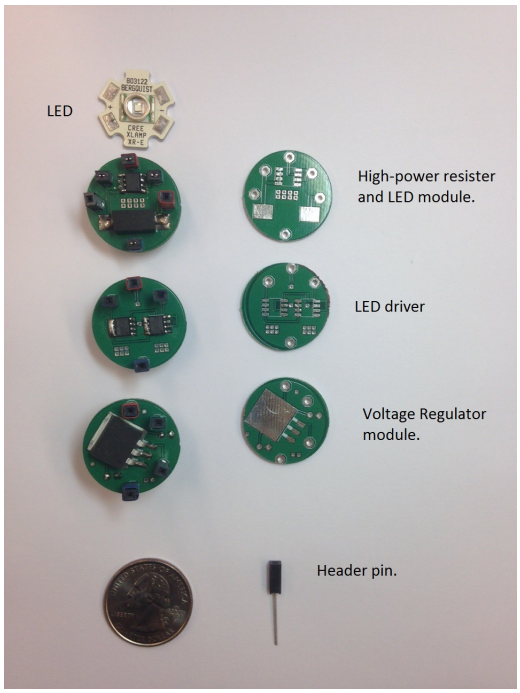

Figure 2.16 Modules of the transmitter circuit.

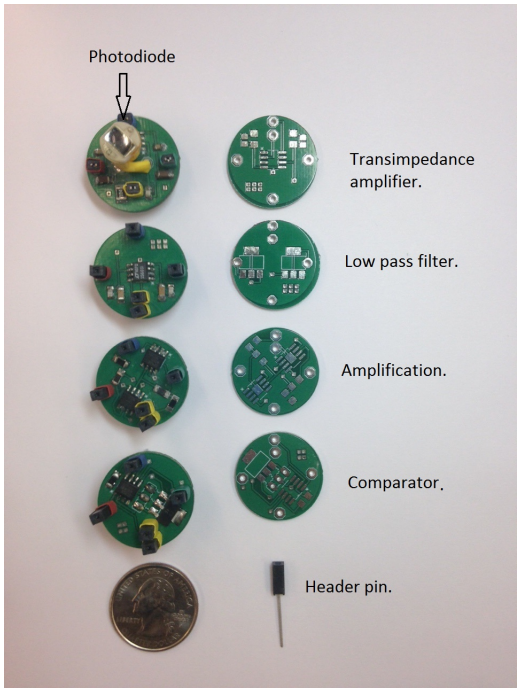

Figure 2.17 Modules of the receiver circuit.

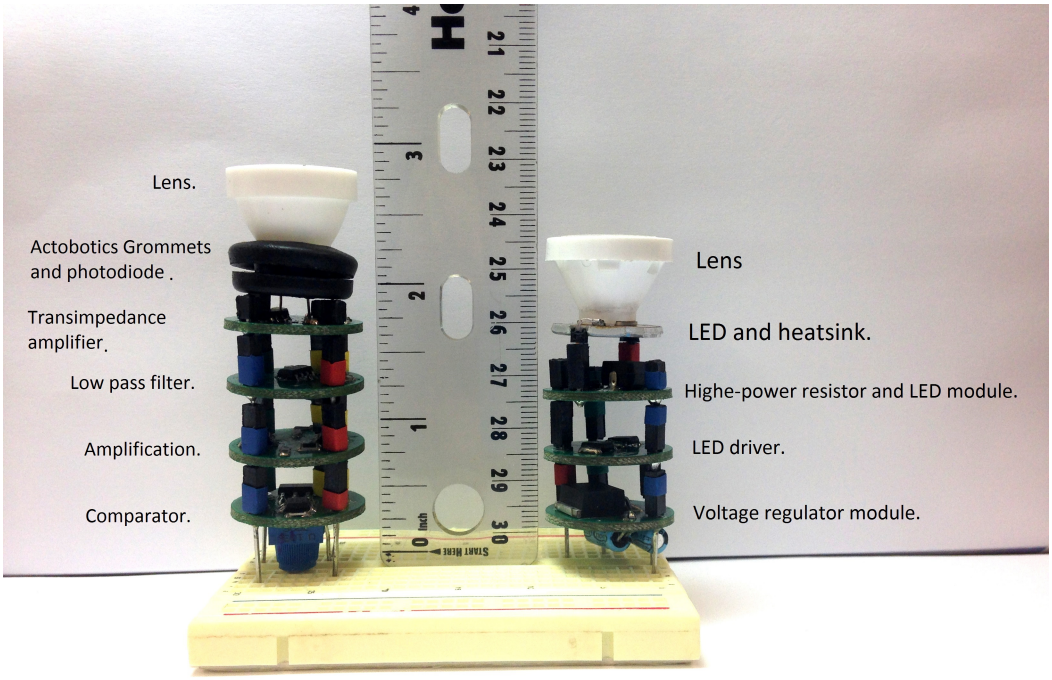

Figure 2.18 The assembled receiver circuit and transmitter circuit, with all modules vertically stacked.

2.4 Rotating Base for the Transmitter/Receiver

Since the optical communication system is designed for use in robots and requires line of sight, it is critical that the orientation of the transmitter and receiver can be adjusted, to maintain communication despite the movement of the underlying robotic platform. For this purpose, a rotating base for the transmitter/receiver has been designed and developed.

2.4.1 Updated Printed Circuit Board and Slip Ring

In order to minimize system complexity and footprint, a new PCB was designed (see Figure 2.19) to hold the components of the receiver and transmitter circuits in one place. It contains two main bards.

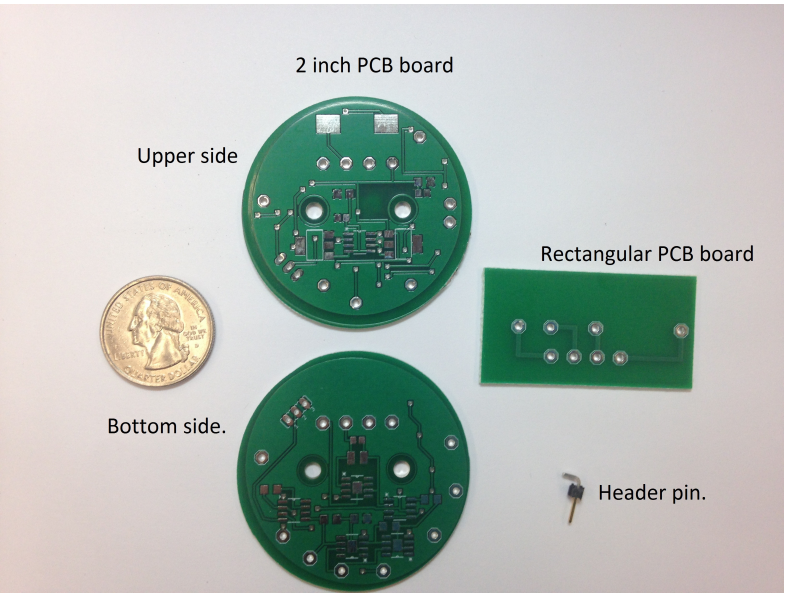

Figure 2.19 Refined PCB design to achieve more compact integration of transmitter/receiver circuits.

The first PCB board is 2 inches in diameter and has two holes in the middle to attach set screw hubs for connecting to a motor shaft. The second PCB board has a rectangular shape with size of 1 inch $\times$ 2 inch, which holds the LED and the photodiode, and it is mounted

perpendicularly to the first circular board by using four 90-degree header pins. The actual boards assembled with components are shown in Figure 2.20.

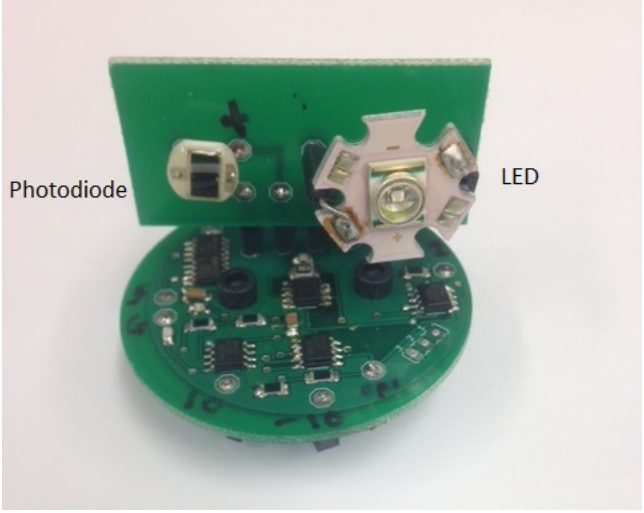

Figure 2.20 Refined transmitter/receiver circuits assembled together.

There are 8 pins in the PCB circuits involving the power supply, the transmitted signal, and the received signal. These pins are connected by wires, which would be twisted when the PCBs are rotated. To address this problem, a slip ring, an electromechanical device that allows the transmission of power and electrical signals from a stationary to a rotating structure, is adopted. A MOFLON MT007 series product (see Figure 2.21) is chosen. This device has color-coded lead wires on both the stator and the rotor for simplified electrical connections. It provides a 12.7 mm through-bore for routing shaft installation, and has a compact outer diameter of 56 mm, featuring long life and fiber brush contact [41].

2.4.2 Actuator and Controller

To rotate the device, a rotational actuator is needed. The actuator must be small, fast and easy to control. For this task, a Precision Micro Drives mini DC motor is used. It is a 12 mm ferrite motor with a spur gear open gearbox, steel geartrain, sintered bronze bearings

Figure 2.21 The slip ring used in this project.

and extra long 65 mm double flat faceted shaft. It is equipped with a shaft encoder, which is instrumental for feedback control of the rotational base for the transmitter/receiver. See Figures 2.22 and 2.23 for the motor/encoder.

To control the DC motor rotation and speed, an Arduino microcontroller connected to a DC motor driver circuit is used. The microcontroller takes commands from the underlying robot to rotate the optical transceiver to specific angles for communication. All these components are integrated together with a 3D-printed frame. Figures 2.24 and 2.25 show the assembly of the device components and the final water-proof package, respectively.

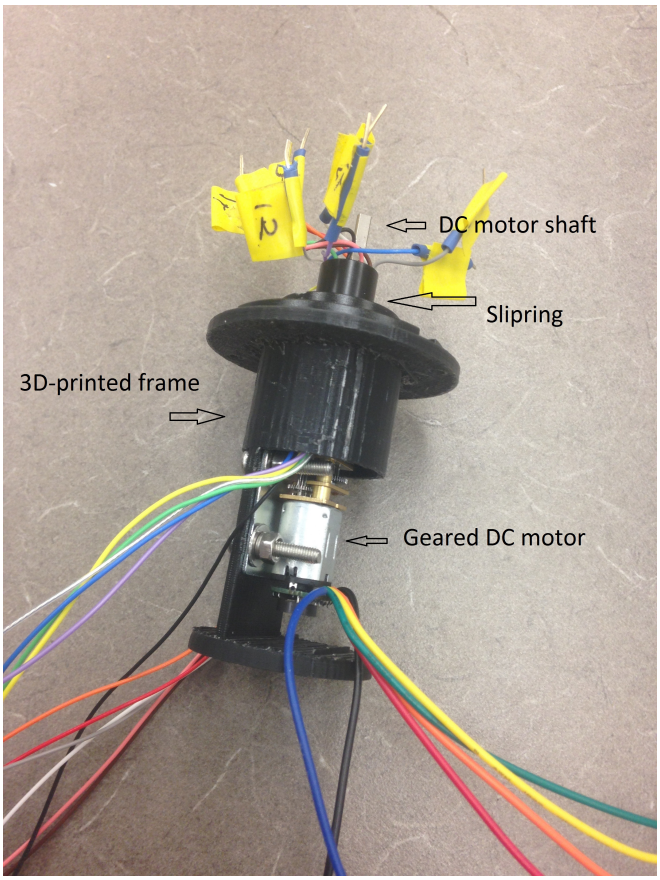

Figure 2.22 The DC motor mounted on a 3D-printed frame.

2.5 Characterization of Optical Communication Link Performance Underwater

In this section we present results from experiments performed in a swimming pool to examine the performance of the optical wireless communication link underwater. The pool length is 23 meter. The transmitter and the receiver are encapsulated in 10 cm-diameter PVC tubes (with transparent window at front) to waterproof them during the underwater experiments. Each of these tubes is then attached to another PVC tube that will fix the depth under the water to 25 cm. The assembly is fixed in the same position with the help of Styrofoam held by a person help. With this configuration, the transmitter and the receiver are underwater

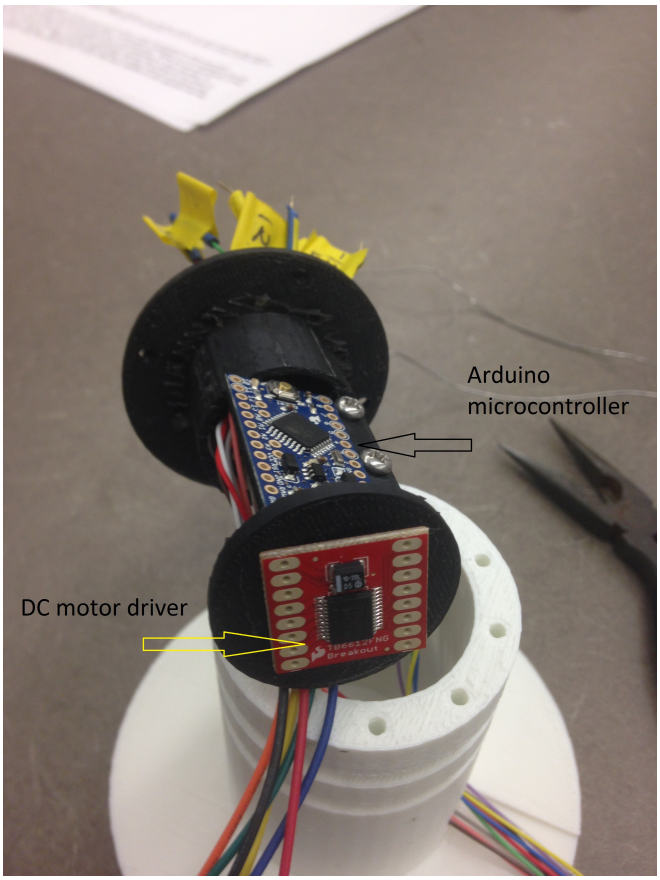

Figure 2.23 The control and driver circuits for the DC motor.

at the same depth and facing each other, as illustrated in 2.26.

The light emitted from an LED spreads over a hemisphere shape. Conditioning optics are required to redistribute the LED light for specific requirements. Lenses are used for that purpose and currently, the most common used LED lens design is the total internal retractor (TIR) lens [42]. In our experiments we use commercially available lens specified for the LED. These lenses come in different viewing angles: (5, 15, 40, 60) degrees. The receiver is also equipped with a 5-degree lens which will help increase the area to receive more photons to obtain stronger signal. For each setting and each distance, experiments are performed five times to mitigate the impact of experimental errors. Figures 2.27-30 show that the signal strength declines when the distance between the receiver and the transmitter

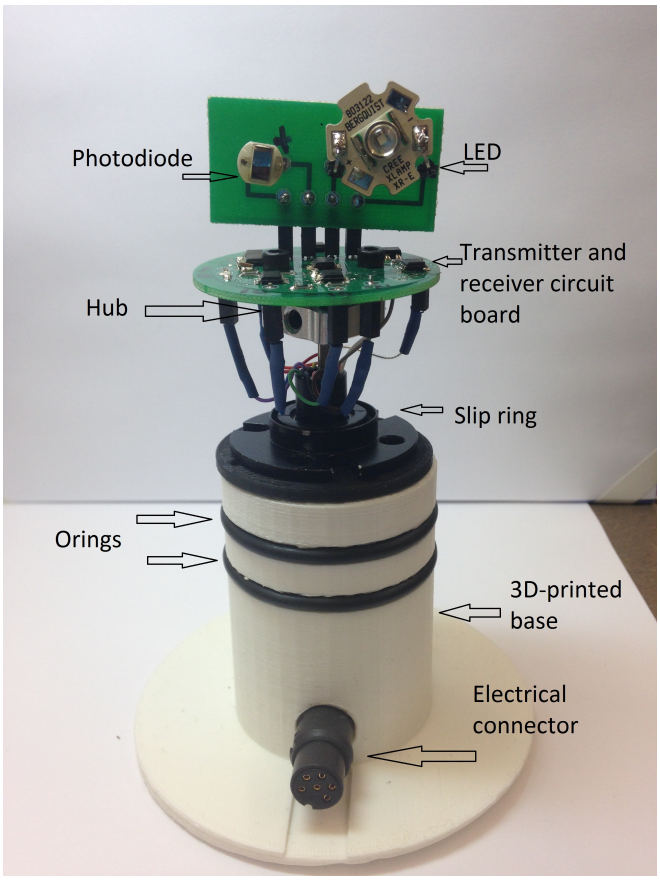

Figure 2.24 The final assembled device without the cover.

increases, for different lens viewing angles for the transmitter; however, there is adequate signal strength (greater than 1 V) throughout the full length of the pool for the designed transmitter/receiver, for the 5 degree case. Here we have used square waves of frequency 10 kHz for the transmitted signal. Figures 2.31 and 2.32 show the output signal after the amplification stage for the distance of 8 meters for the frequency of 10 kHz and 100 kHz, respectively. From these figures, we can see that the signal largely maintains the shape of a square wave at least up to the frequency of 100 kHz. Such minimal waveform distortion is instrumental in reducing the bit error rate in communication. The final design the transmitter and the receiver were equipped with 5 degree lenses.

In addition to the signal strength measurements, we have also examined the data trans-

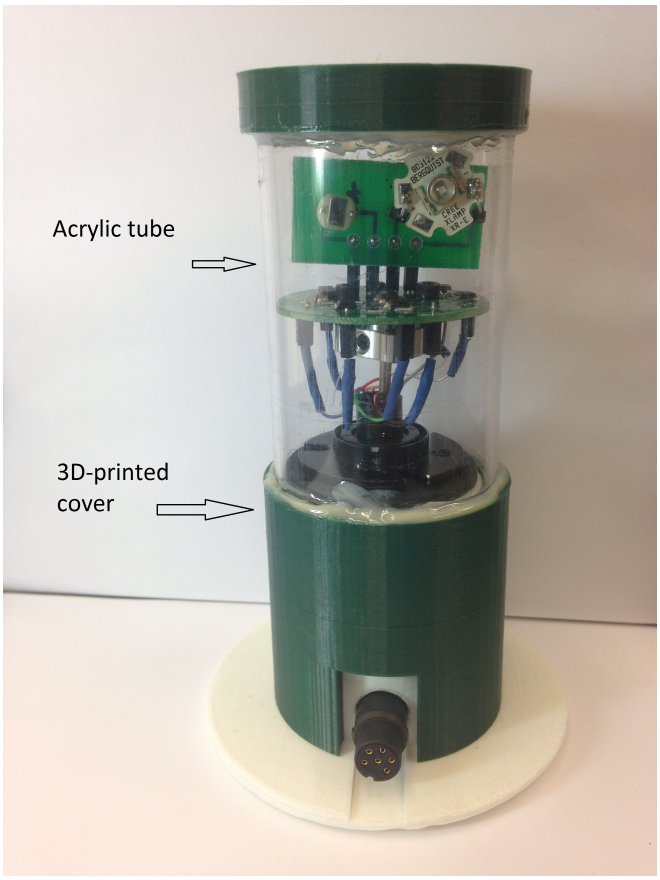

Figure 2.25 The final assembled device with the cover.

mission performance of the system underwater. In the experiments, we use two computers to emulate two underwater robots and we connect them to the transmitter and the receiver respectively, from the USB port using the FT232R USB-TTL level serial converter cable. The cable uses an FT232RQ chip, housed in the USB connector, to convert USB data into asynchronous serial data at TTL levels. We send over 270,000 bytes five times at a distance of 22 m and receive those bytes on another computer. We confirm that the system will transmit and receive at a speed of 115.2 Kbps with a bit error rate (BER) of zero. Figure 2.33 shows an example of the received signal waveform.

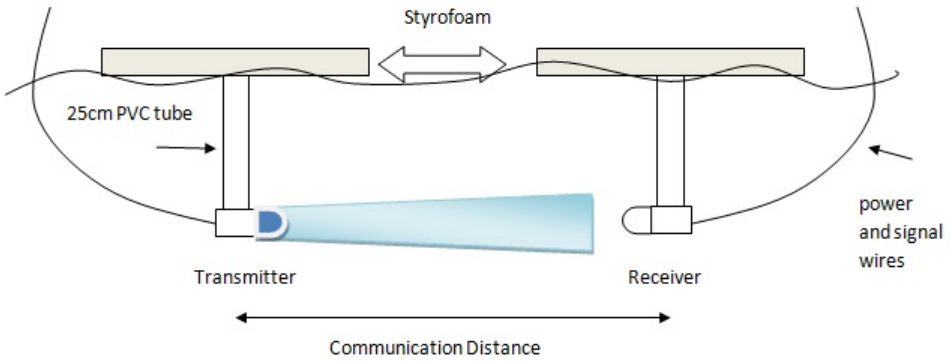

Figure 2.26 Schematic of the setup for swimming pool experiments.

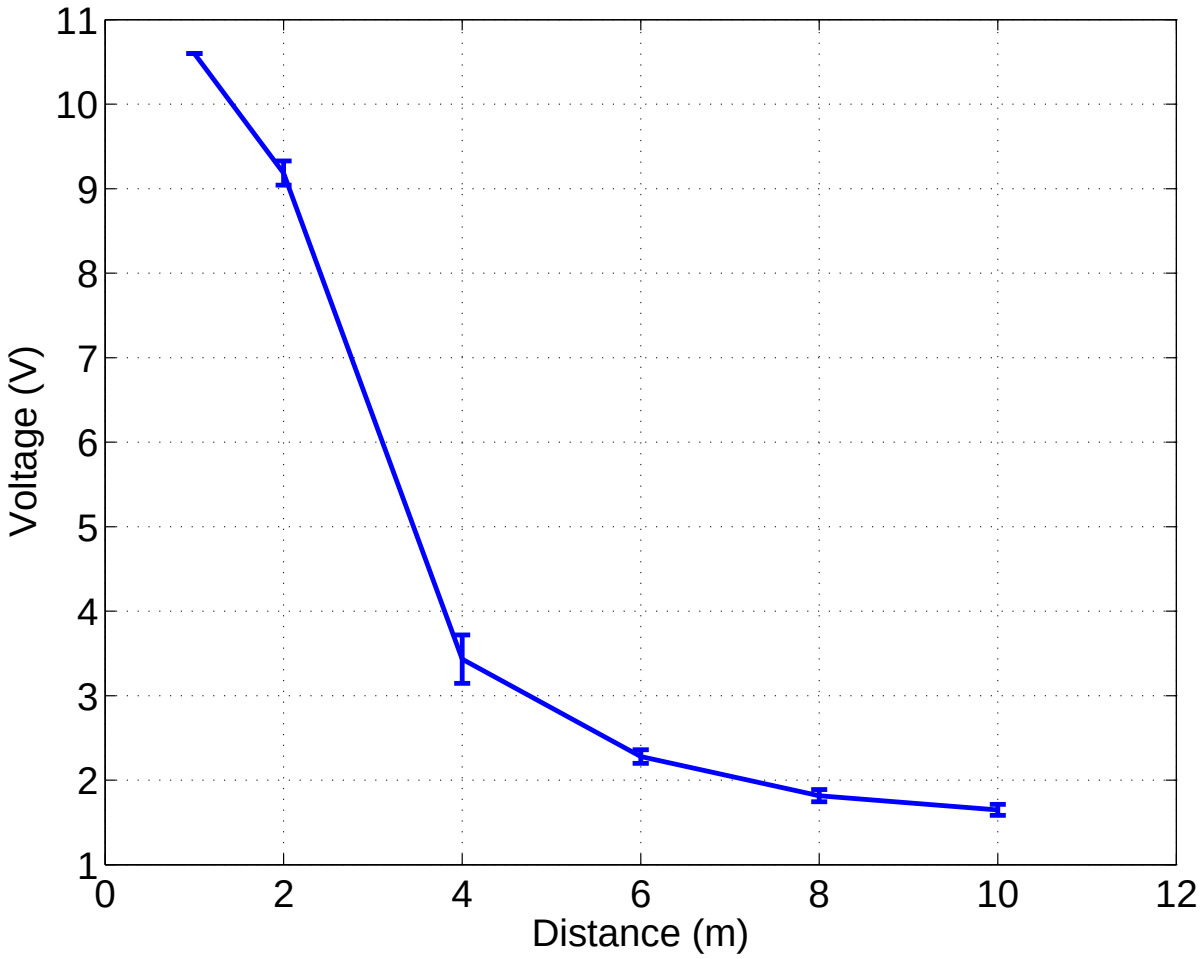

Figure 2.27 The measured signal strength versus the transmitter-receiver distance in swimming pool experiments for the case of 60-degree lens for the transmitter.

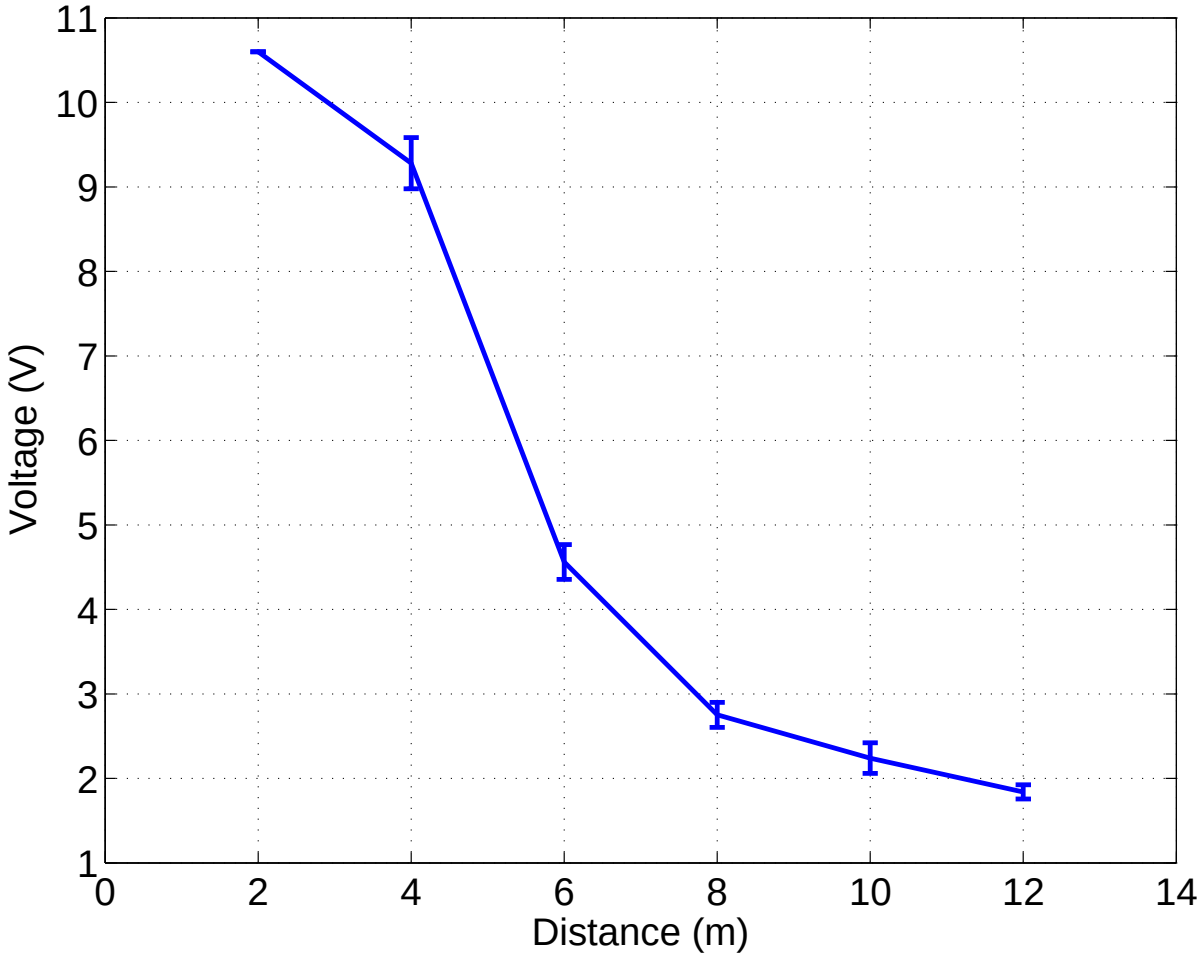

Figure 2.28 The measured signal strength versus the transmitter-receiver distance in swimming pool experiments for the case of 40-degree lens for the transmitter.

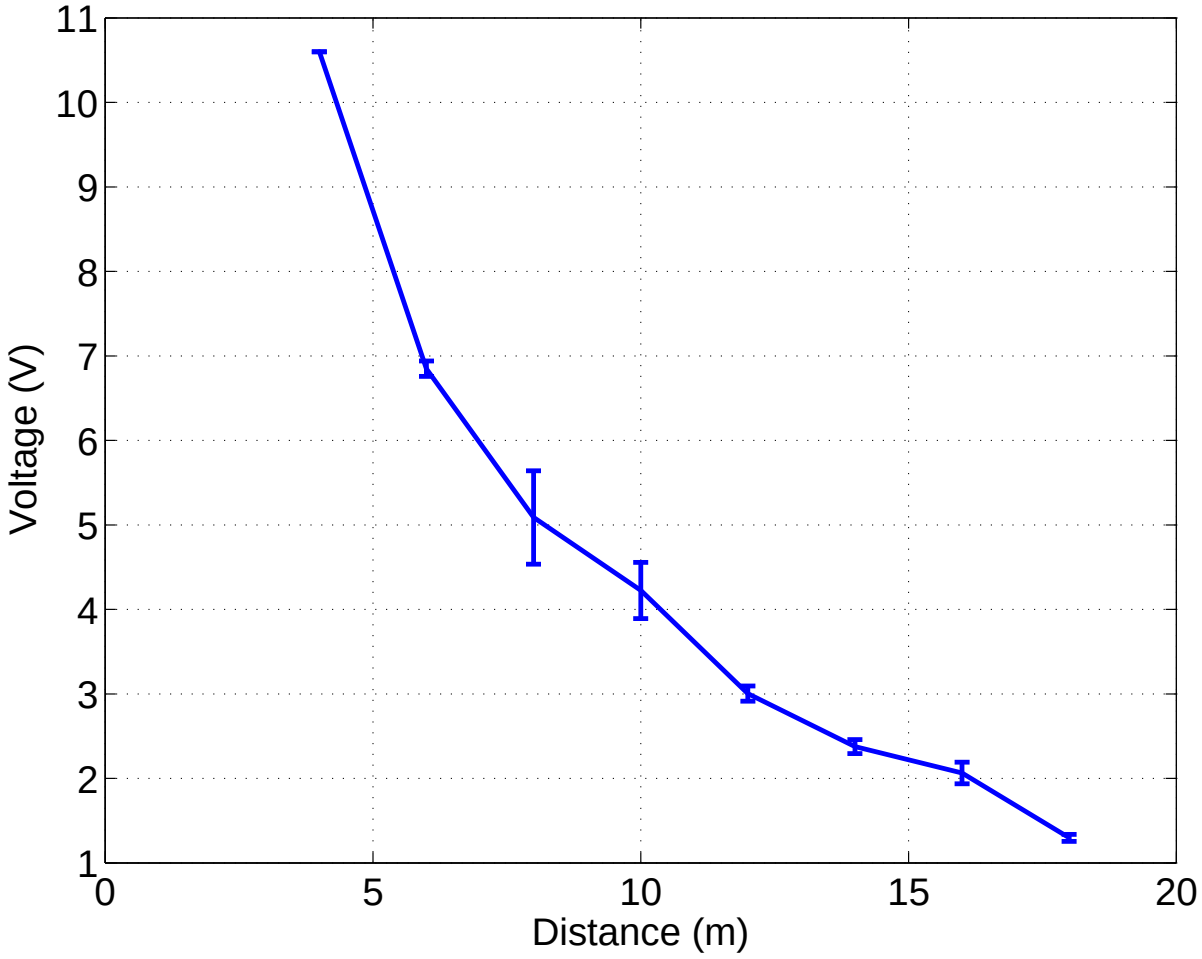

Figure 2.29 The measured signal strength versus the transmitter-receiver distance in swimming pool experiments for the case of 15-degree lens for the transmitter.

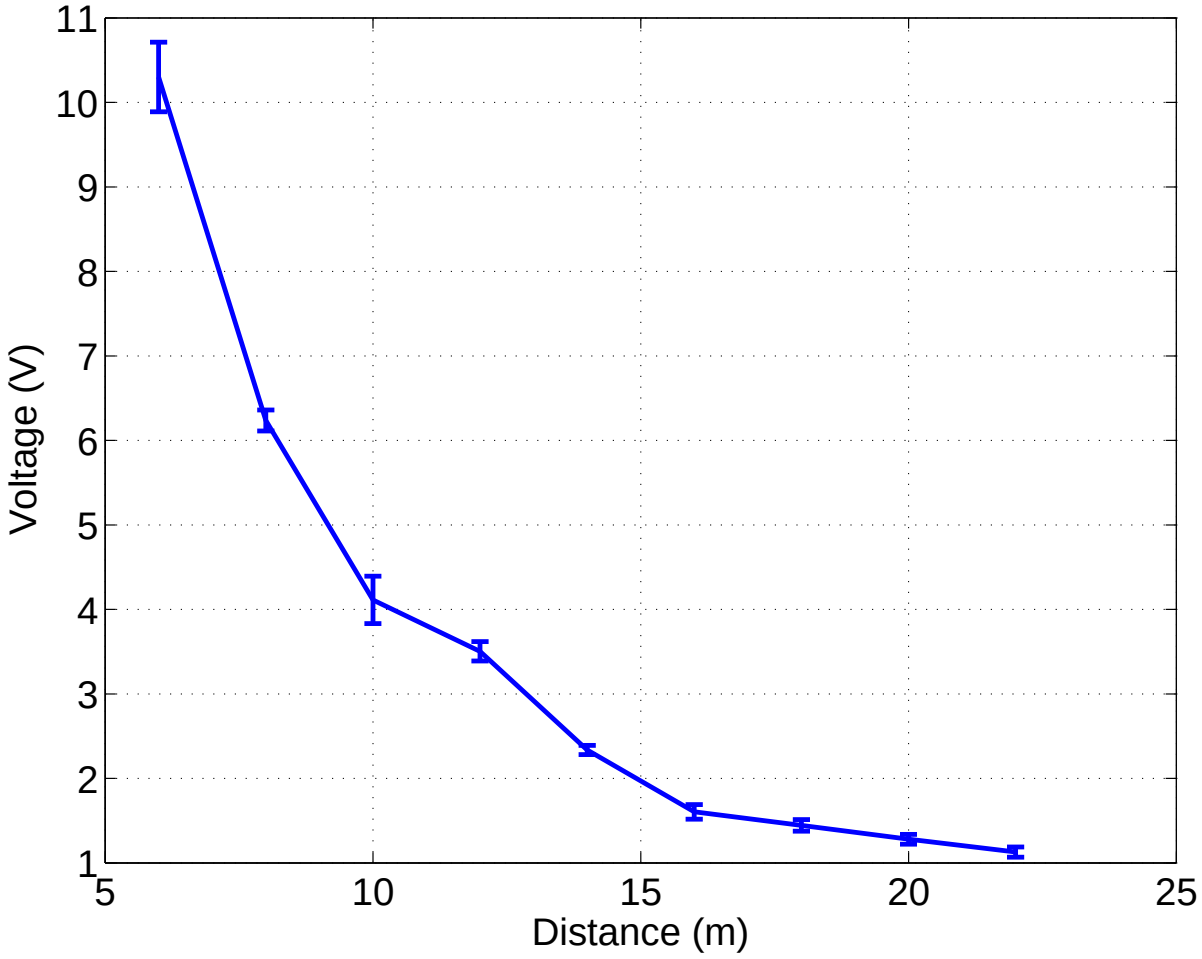

Figure 2.30 The measured signal strength versus the transmitter-receiver distance in swimming pool experiments for the case of 5-degree lens for the transmitter.

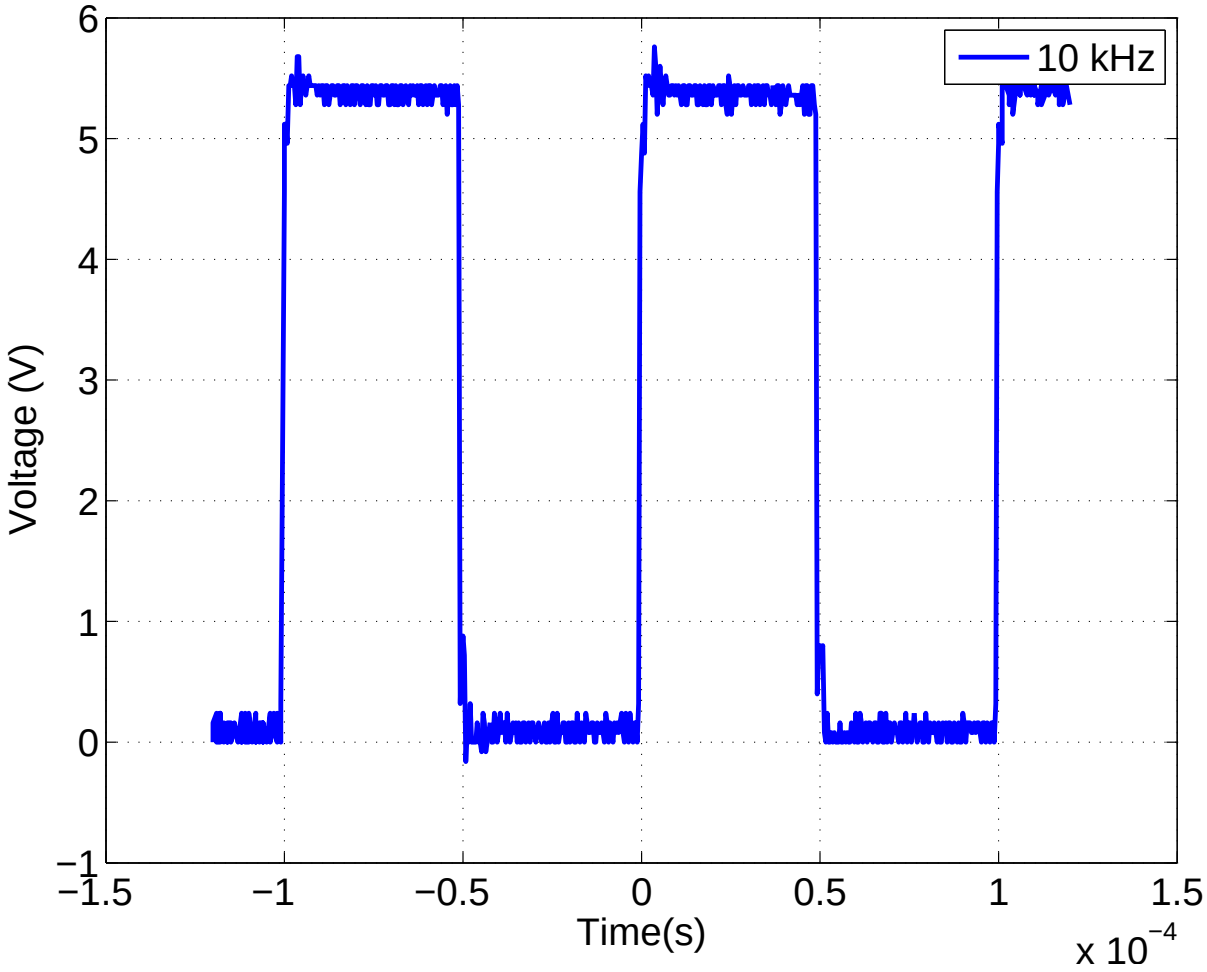

Figure 2.31 Measured signal waveform with 10 kHz frequency for a 5-degree viewing angle LED, measured at a distance of 8 meters.

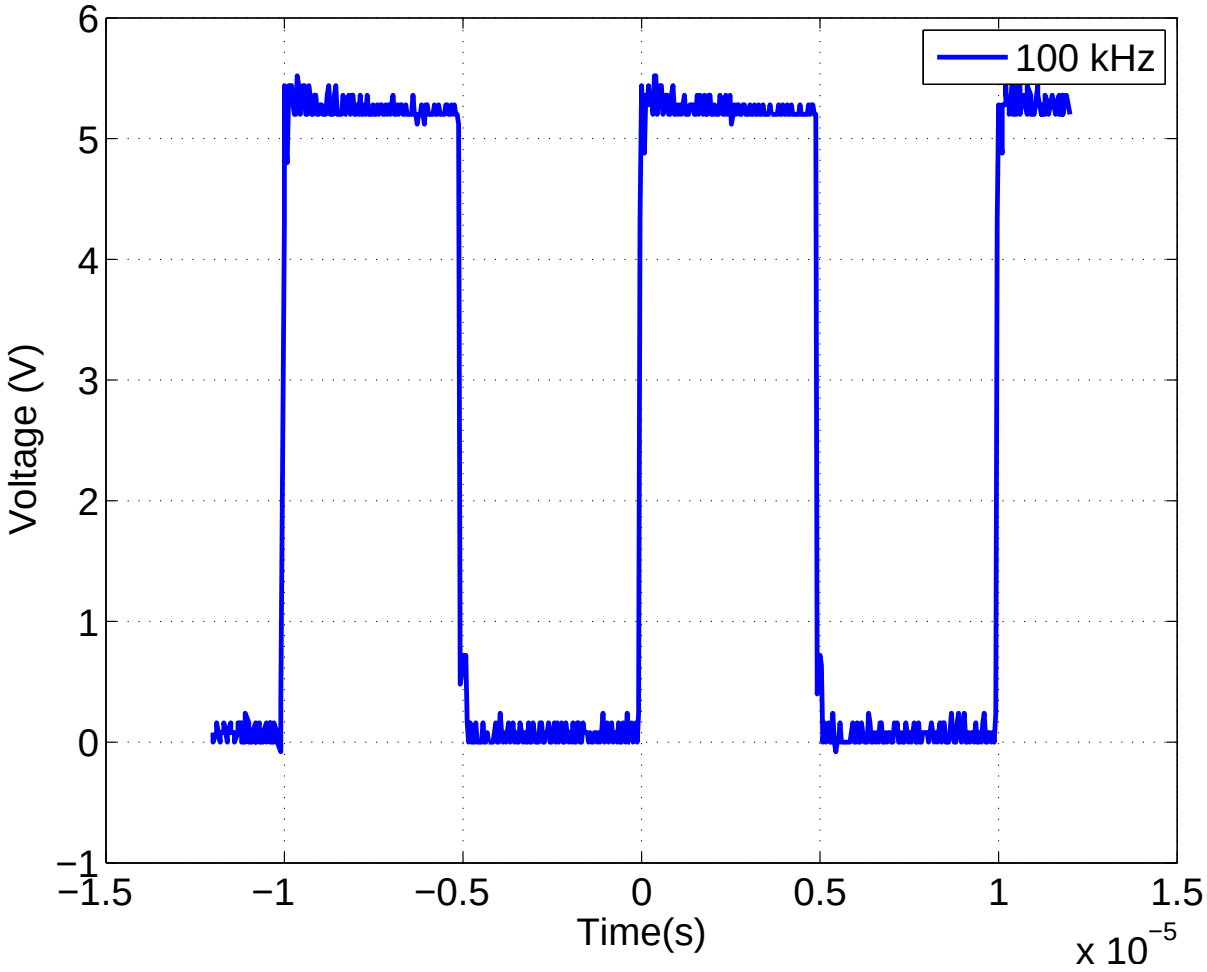

Figure 2.32 Measured signal waveform with 100 kHz frequency for a 5-degree viewing angle LED, measured at a distance of 8 meters.

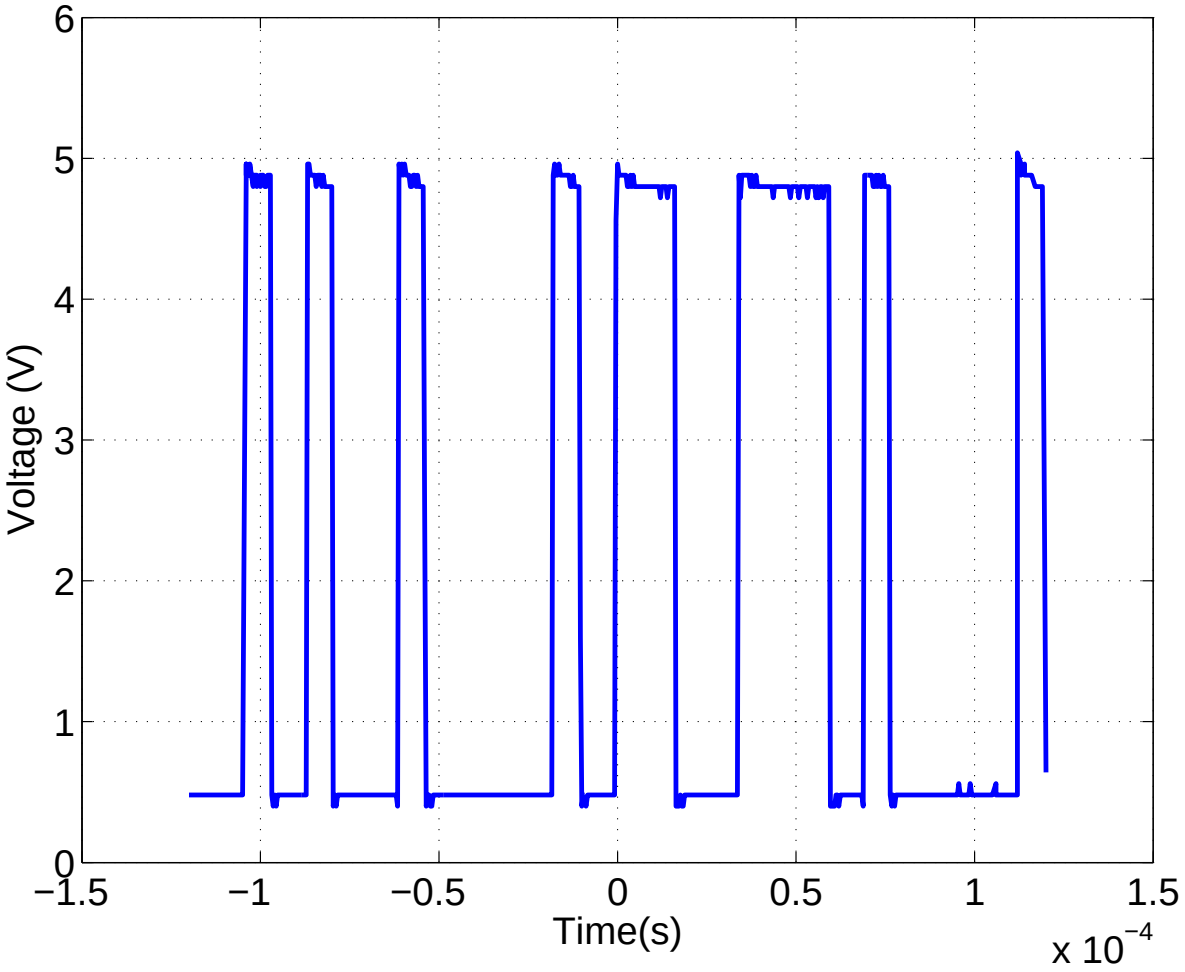

Figure 2.33 The signal waveform captured during the communication bit error tests at a baud rate = 115200 bps.

Chapter 3

Optical Communication Signal Strength Model

In this chapter a mathematical model is presented for capturing the signal strength in a wireless optical communication system. Such a model will be instrumental in developing the estimation and control algorithms in alignment maintenance of optical communication systems when the underlying platforms are mobile. Such a model can also provide insight into design considerations for improving the communication performance.

3.1 Mathematical Model

The model used is derived from [43] with some tweaking to fit our device. The model allows us to compute the power or signal strength arriving from the light source to the optical detector. The model includes the following stages of the transmitter and receiver circuit, including LED, photodiode, and transimpedance amplifier. And no extra lens are used in this model description. The model mainly describes the effect of the relative position and orientation between the transmitter and the receiver on the signal strength. Refer to Figure 3.1. For the chosen hardware configuration, the model computes the received power as a function of transmission angle θ, transmission distance d, and reception angle ϕ.

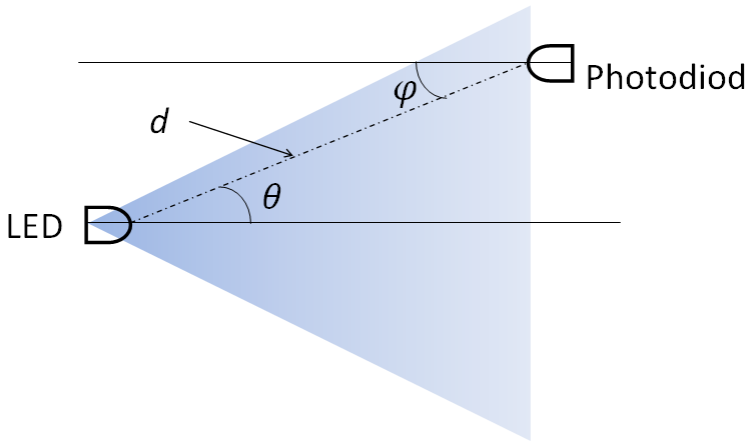

Figure 3.1 Illustration of the relative position and orientation between the transmitter and the receiver.

3.1.1 Transmitter Optical Power

The transmitter light source used is Cree XR-E Series Blue Lighting LED. The LED datasheet provides us with the spatial intensity distribution of the LED. Basically it is the measurement of the light intensity at varying angles from the LED's normal direction. This angular intensity distribution is rotationally symmetric about the LED's normal. If we know the intensity of the LED along the normal to the LED ($\theta = 0$), we can determine the intensity at various angular points by the use of this spatial intensity curve. The typical relative intensity graph for this LED is shown in Figure 3.2. We use a summation of three Gaussian functions to fit the data from the datasheet

$$f(\theta) = a_1 e^{\frac{-(\theta-b_1)^2}{2\sigma_1^2}} + a_2 e^{\frac{-(\theta-b_2)^2}{2\sigma_2^2}} + a_3 e^{\frac{-(\theta-b_3)^2}{2\sigma_3^2}} \tag{3.1}$$

The parameters $(a_1, a_2, a_3, b_1, b_2, b_3, \sigma_1, \sigma_2, \sigma_3)$ are found by using a curve-fitting toolbox in Matlab software which uses the method of least squares. To express the radiant intensity I_θ, for a given angular displacement θ, we use Eq. (3.2), where $f(\theta) \in [0, 1]$ and the maximum

intensity $I = 0.038$ W/sr [43].

$$I_\theta = I f(\theta) \tag{3.2}$$

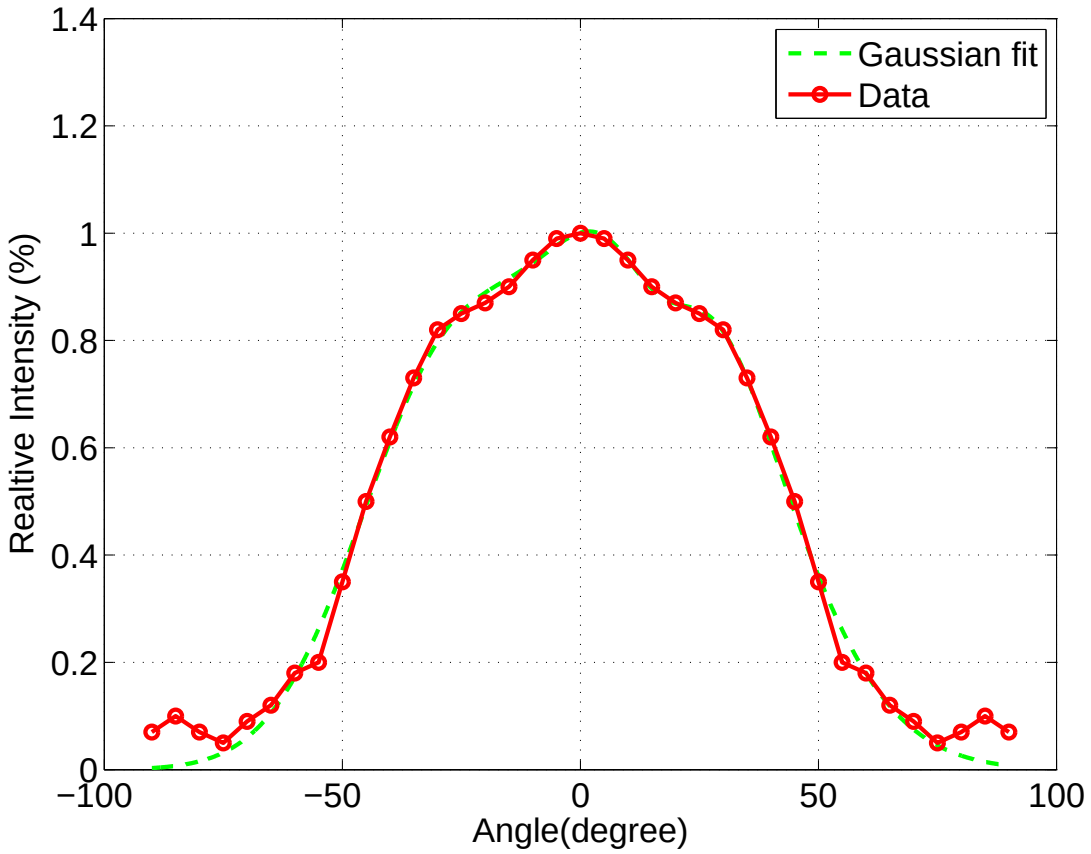

Figure 3.2 Relative intensity of LED [7] (red) and Gaussian fit (green). The x-axis shows the angular displacement in degrees, the y-axis shows the relative intensity in percent.

3.1.2 Light Detector Sensitivity

A spherical spreading model with exponential decay is considered in this work. In clear water, where scattering does not play a crucial role, this model works well. First, we consider power loss due to spherical spreading. Let d be the distance in [m] at which we measure the signal intensity. Using the intensity I_θ from Equation (3.2), we get irradiance E_θ which is the

radiant flux received by a surface per unit area at distance d, measured in $\mathrm{W/m^2}$:

$$E_\theta(d) = I_\theta / d^2 \tag{3.3}$$

To describe the extinction of the light signal we will use Beer's Law [44], which is used in understanding the attenuation in physical optics. Let c be the attenuation coefficient for the medium in which the light transmits. We assume that the coefficient is uniform across the entire length of transmission. Beer's law gives the signal degradation at distance d caused by absorption as

$$A = e^{-cd} \tag{3.4}$$

By combing the effect of spherical spreading with exponential decay, we get a final irradiance equation of

$$E_\theta(d) = I_\theta e^{-cd} / d^2 \tag{3.5}$$

The incident power can be computed from the signal irradiance arriving at the detector Eq.(3.5), the incident angle ϕ, and the area A_0 (assumed flat) of the detector:

$$P_{\text{in}} = E_\theta(d) A_0 \cos(\phi) \tag{3.6}$$

For a given sensor, the relationship between the incident power and the current output, called responsivity, can be captured with a linear gain R_d. So the photodiode output current is expressed as

$$I_d = R_d P_{\text{in}} \tag{3.7}$$

The current produced by the photodiode must be amplified and converted into a voltage before it can be processed by the analog to digital converter. This is typically done using a transimpedance amplifier (TIA). The gain of the amplifier is set by the feedback resistor and at low frequencies the feedback capacitor has little effect on the amplifier response as shown in Figure 3.3.

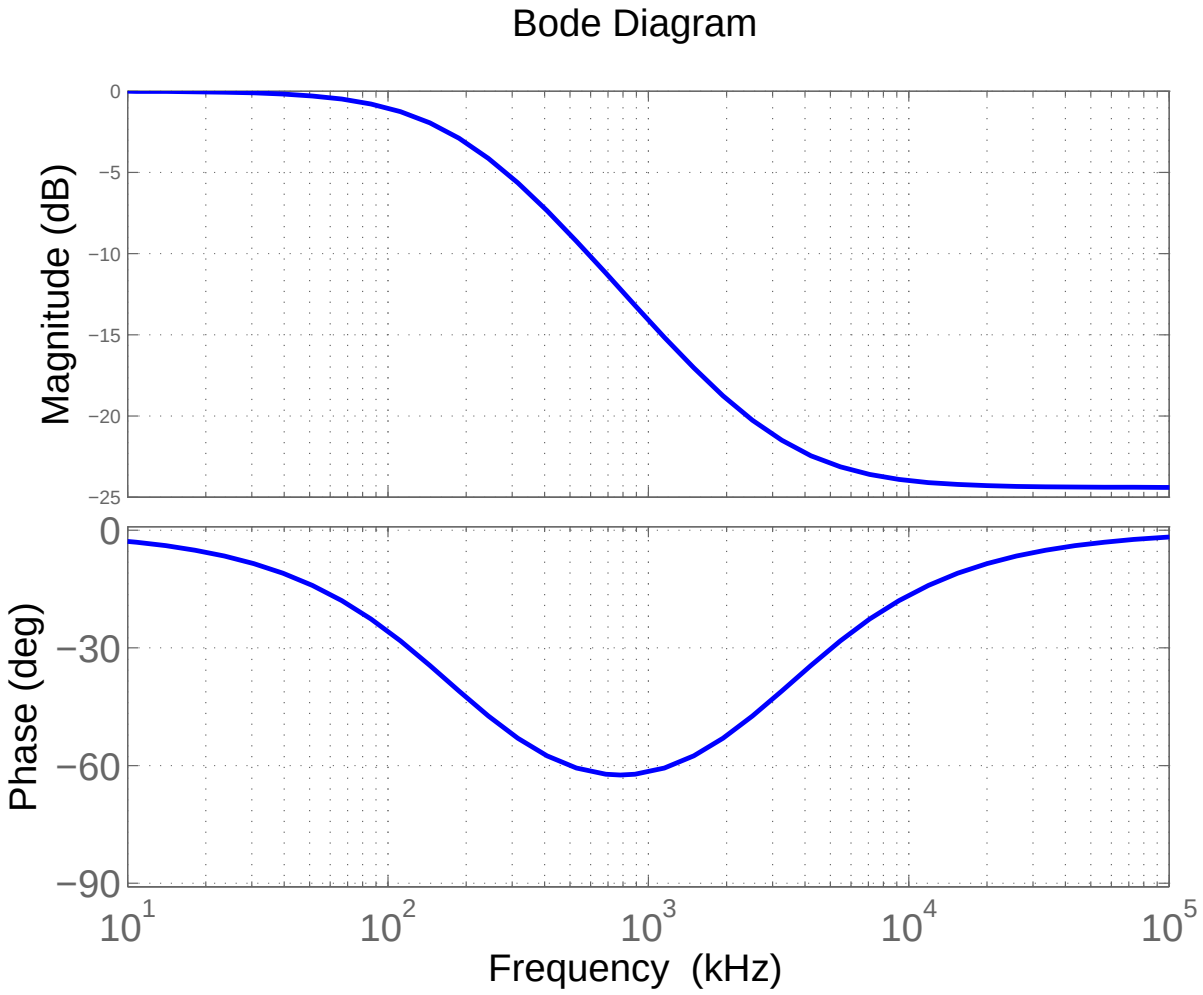

Figure 3.3 Frequency response of the transimpedance amplifier.

The amplifier response is close to the ideal, and the current is converted into a voltage as

$$V_d = R_f I_d \tag{3.8}$$

The full signal strength model can then be summarized as

$$V_d = C I_\theta e^{-cd} \cos(\phi)/d^2 \tag{3.9}$$

where $C = A_0 R_d R_f$ is a scaling constant.

3.2 Experimental Model Identification and Validation

Three experiments are presented in this section. The first experiment is used to find the parameters for model (3.9) when only the distance d is changed. The second one is for a fixed communication distance while the receiver angle ϕ is changed, and the last one is for a fixed communication distance while the receiver angle θ is changed. Note that all these experiments are conducted in air.

In the experiments, a one-inch 80/20 frame and some steel plates are used to construct a sliding mechanism with a travel distance of 2 m; see Figure 3.4. The transmitter and the receiver circuits are fitted inside a PVC tub to facilitate attaching them to the steel plates with clamps. The mounting angles of the receiver and the transmitter are variable in the horizontal plane, to allow an arbitrary choice of the rotation angles for both.

3.2.1 Model Identification

The only unknown parameters in the model (3.9) are C and c. In order to estimate these parameters, both the transmitter and the receiver are set to aim directly at each other

($\theta = \phi = 0^\circ$). Then the transmitter is moved to a fixed distance, where we acquire the signal strength value (the voltage output at the receiver side). The range of distances used for these experiments is 10 cm to 150 cm in increment of 10 cm. The measurements and the model with different displacement d are shown in Figures 3.5. The data from the first case, where ($\theta = \phi = 0^\circ$) are used to find the parameters in (3.9). Using the curve fitting toolbox in Matlab software, C is found to be 2.099 and c is -0.8665.

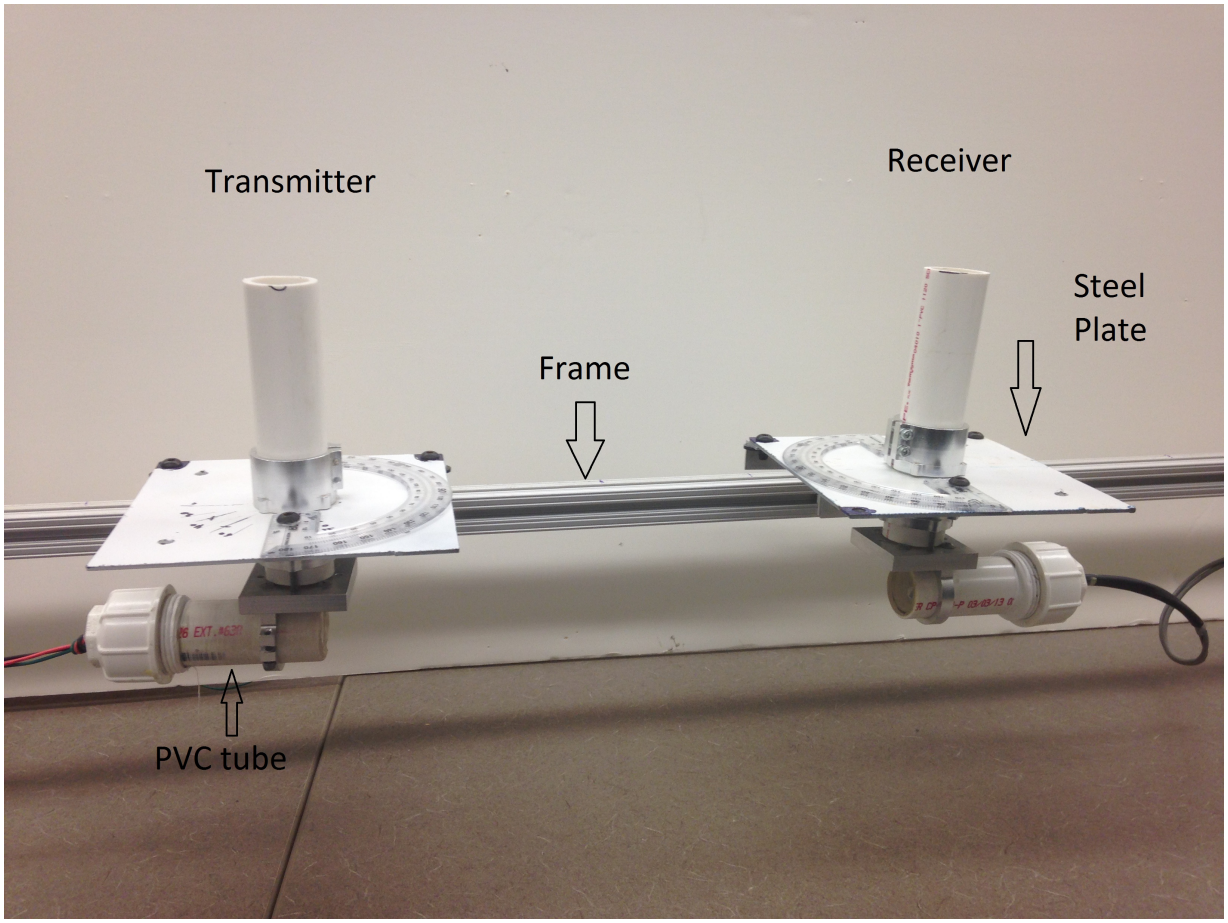

Figure 3.4 Experimental setup for the identification and validation of the signal strength model in air.

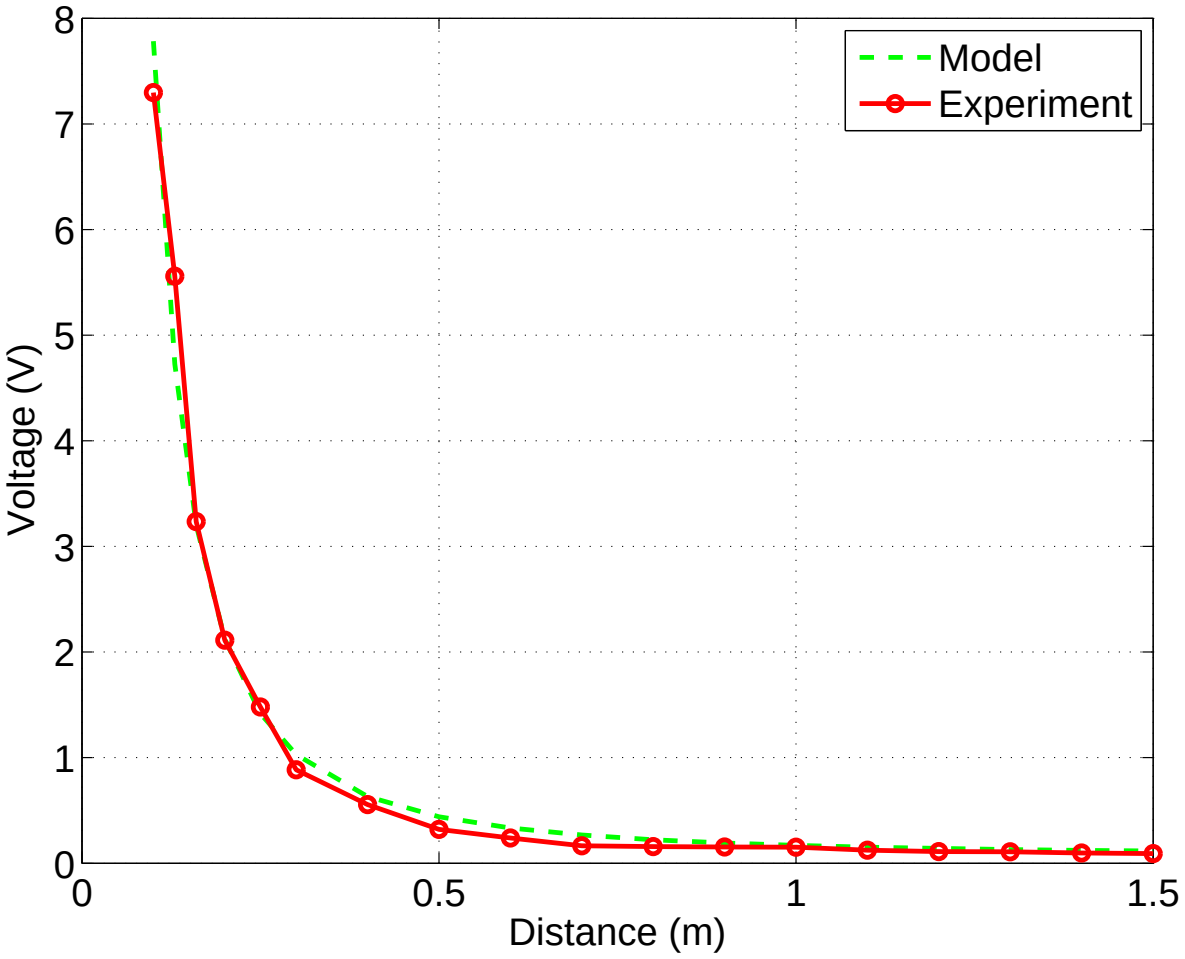

Figure 3.5 Modeled signal strength and experimental data. The green line shows the output of the model.The experimental data is plotted in red and ($\theta = \phi = 0^\circ$)

3.2.2 Model Validation

First we validate the model is able to predict the signal strength at different receiver angles. The emitter angle is fixed at $\theta = 0^\circ$ and the distance is fixed at 20 cm. The range of rotation for the receiver is from 0° to 70°. The measurements and the model predictions with different receiver angle ϕ are shown in Figures 3.6. It can be seen that the model fits the experimental data well; in particular, the cosine function is able to capture the dependence of the signal strength on the receiver angle.

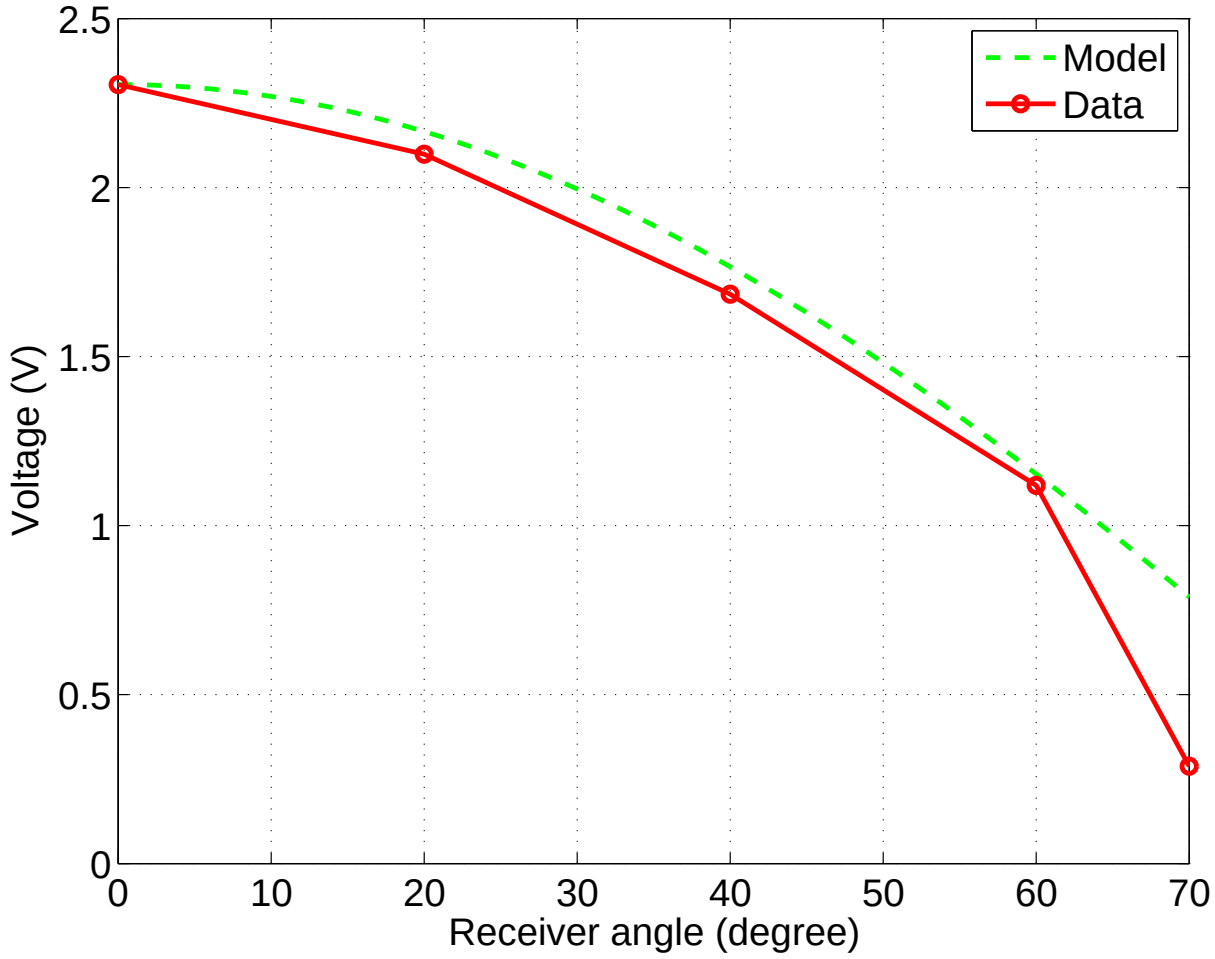

Figure 3.6 Experimental validation of the signal strength model as the receiver angle varies. Here the distance is fixed at 20 cm.

Next we verify the model is able to capture the dependence of the signal strength on the

emitter angle. In particular, we would like to validate Eq.(3.1). The receiver angle is fixed at ($\phi = 0\ ^\circ$) and the distance is fixed at 20 cm. The range of the emitter rotation is from 0° to 70°. Good match is achieved between the signal strength measurements and the model predictions, as shown in Figure 3.7.

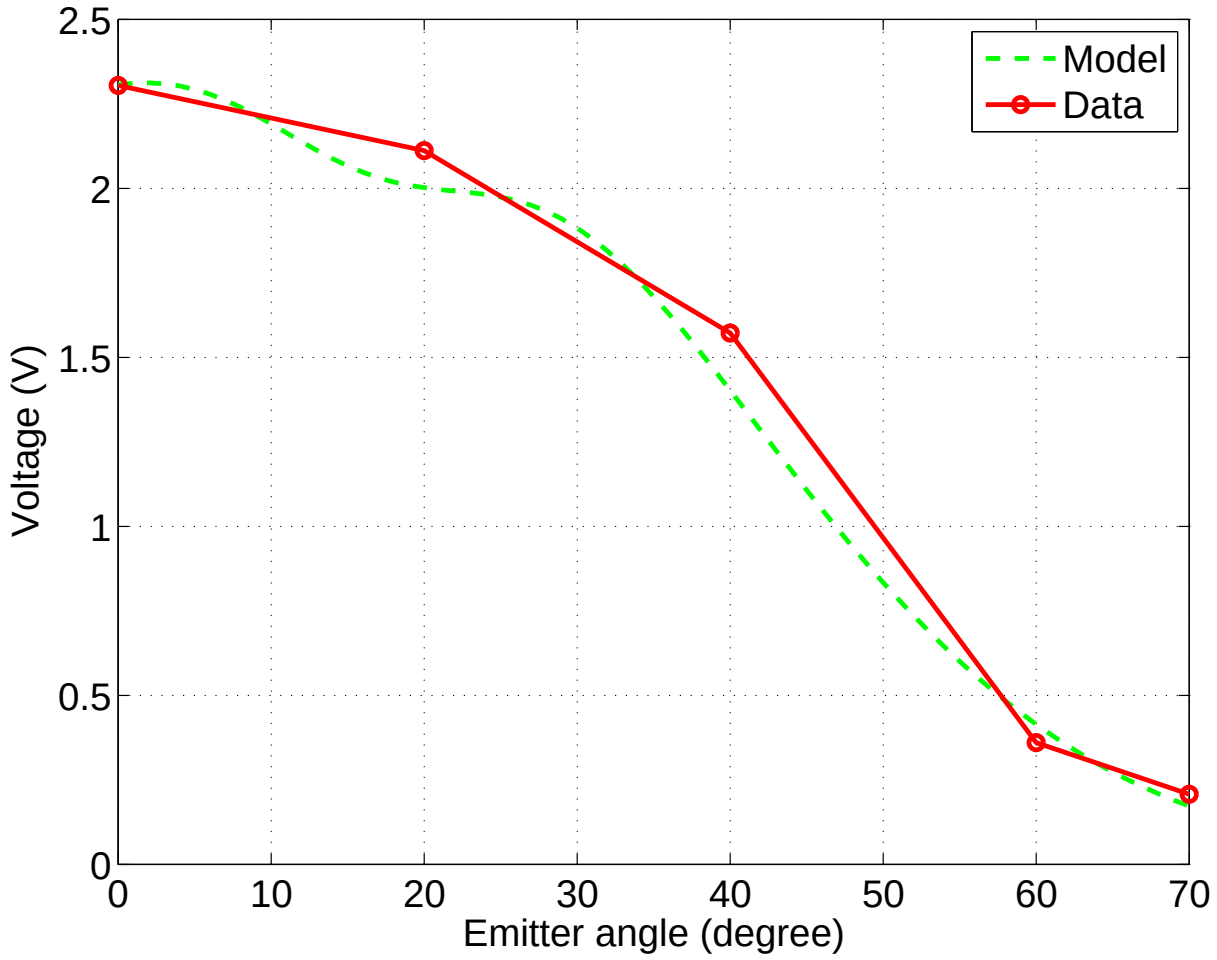

Figure 3.7 Experimental validation of the signal strength model as the receiver angle varies. Here the distance is fixed at 20 cm.

Finally, to validate the complete model described in (3.9), multiple experiments are conducted for variable tramitter and receiver angles along with the variation of distance. Comparisons shown in Figures 3.8-3.11 show consistency between the model predictions and experimental measurements.

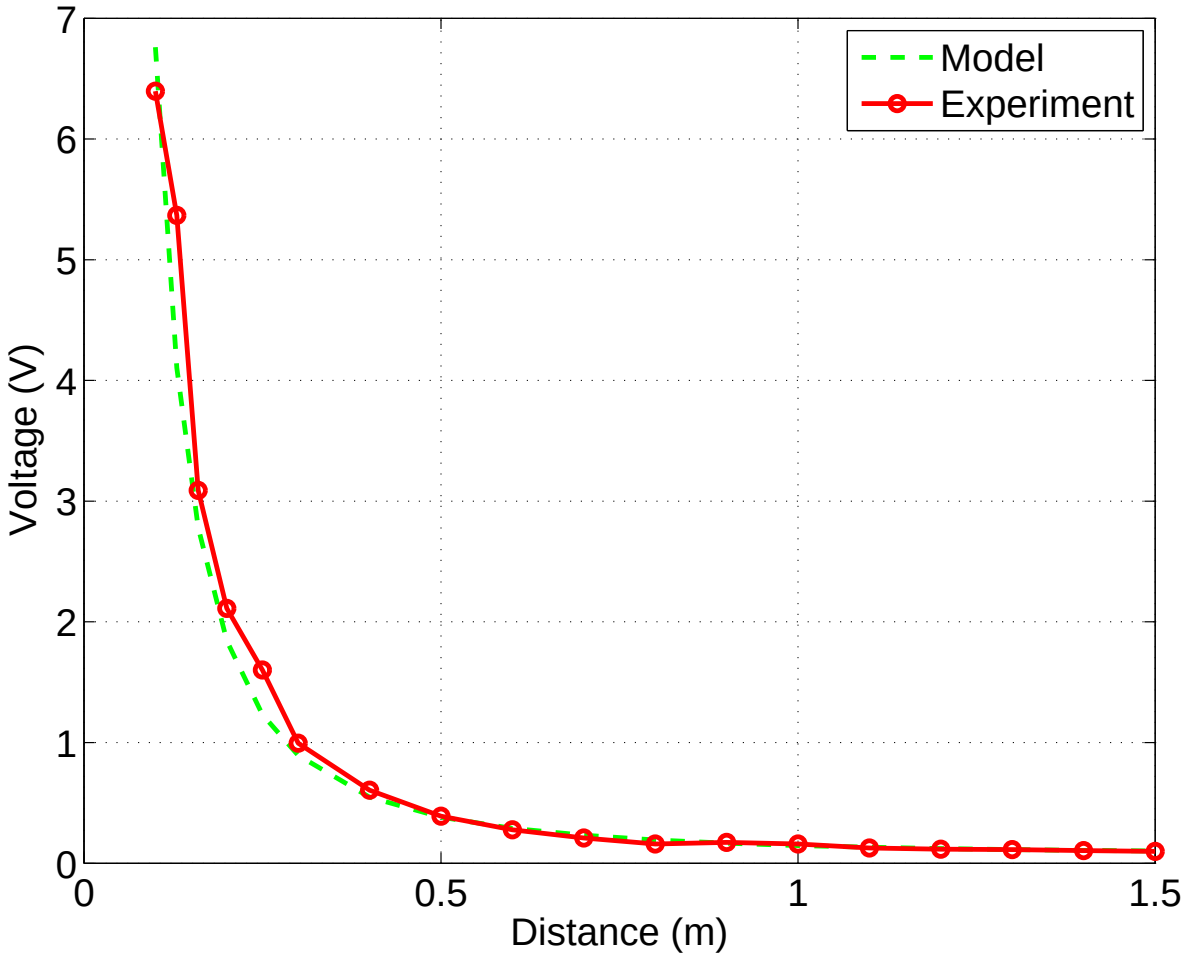

Figure 3.8 Experimental validation of the signal strength model with transmission angle $\theta = 20\ ^\circ$ and reception angle $\phi = 0\ ^\circ$.

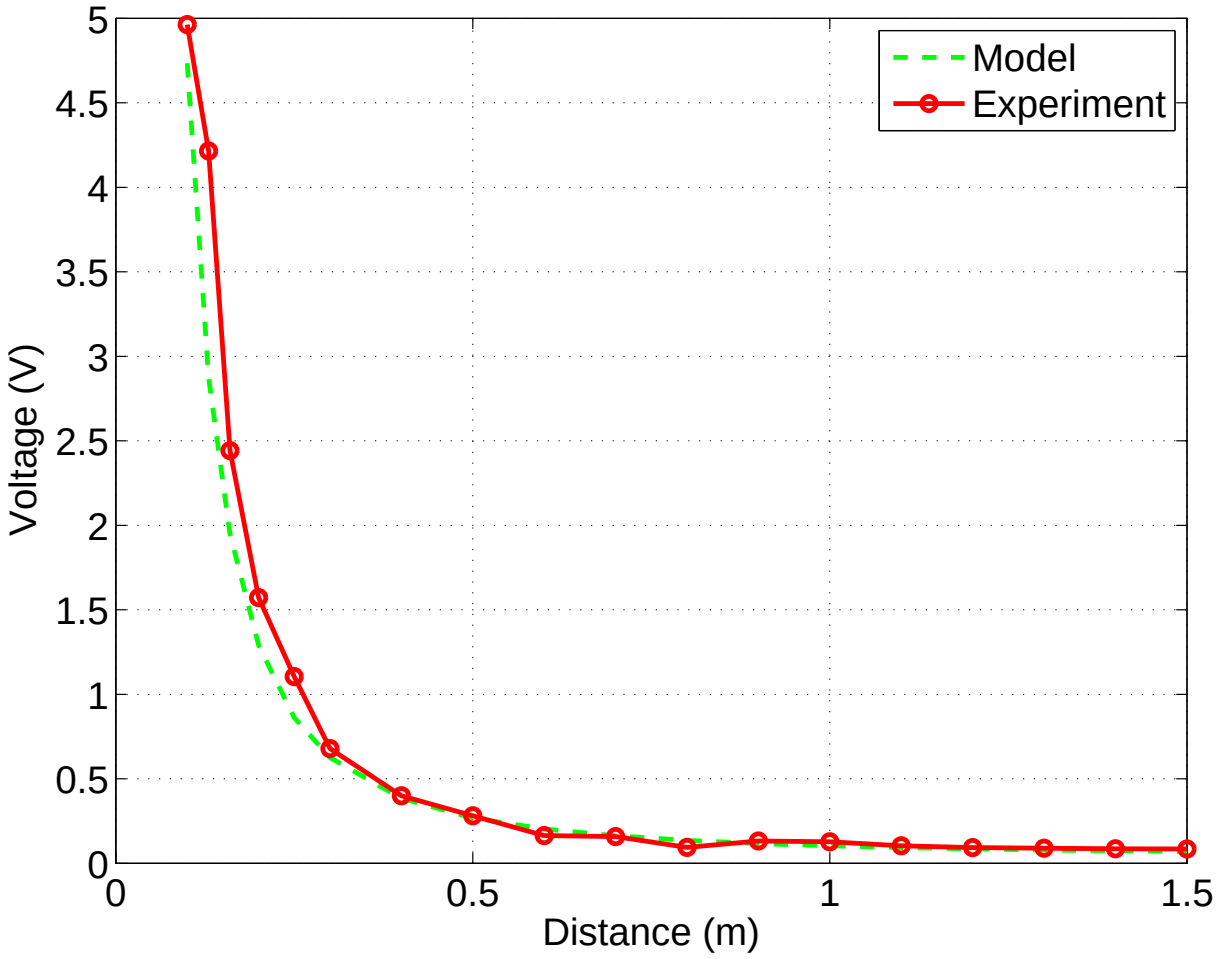

Figure 3.9 Experimental validation of the signal strength model with transmission angle $\theta = 40\ ^\circ$ and reception angle $\phi = 0\ ^\circ$.

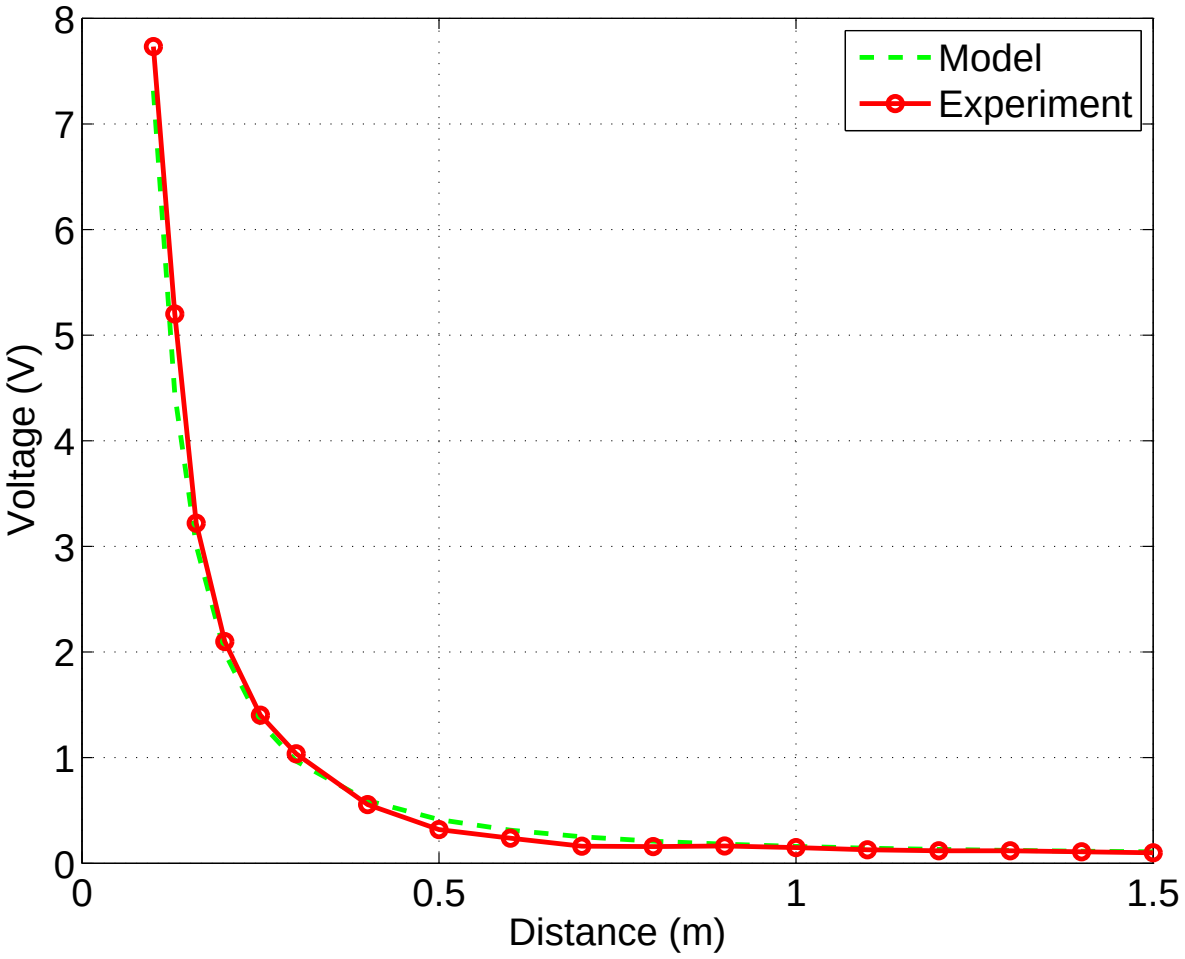

Figure 3.10 Experimental validation of the signal strength model with transmission angle $\theta = 0\ ^\circ$ and reception angle $\phi = 20\ ^\circ$.

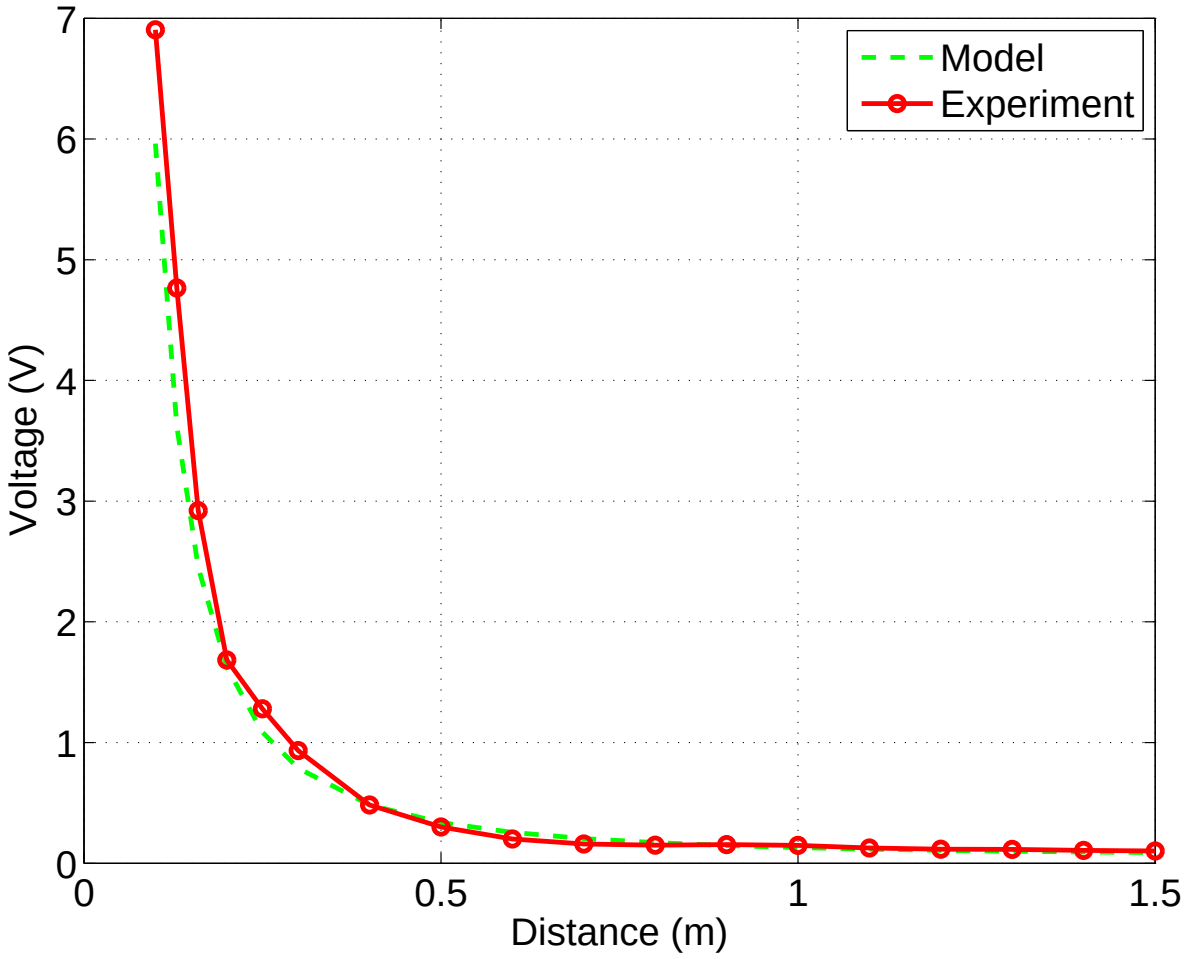

Figure 3.11 Experimental validation of the signal strength model with transmission angle $\theta = 0\ ^\circ$ and reception angle $\phi = 40\ ^\circ$.

Chapter 4

Active Alignment Control System

In this chapter, we present an active control algorithm for maintaining the alignment of the receiver with the transmitter for LED-based communication systems, in the presence of the underlying movement of the robotic carriers. The algorithm uses the received signal strength as feedback for adjusting the receiver angles. The effectiveness of this approach has been demonstrated in experiments involving a mobile robot (receiver) and a stationary transmitter.

4.1 Tracking Algorithm

The proposed algorithm aligns the rotating base on the receiver end to the LED light. In particular, it uses the signal strength to guide the movement of the rotating base, so that sufficient signal strength is maintained despite the movement of the transmitter. The details of the algorithms are as follows:

1. When the tracking is initiated, the analog signal from the receiver circuit is measured.

2. The rotating base keeps rotating until it senses a voltage signal higher than the threshold voltage.

3. After the communication has started, the algorithm keeps checking the voltage signal, and when the value drops under the threshold (1 Volt), the base starts a search function.

4. The search function (see Figure 4.1) will perform a clockwise rotation and then a counter-clockwise rotation for an angle ψ from the original location , and it will take the voltage measurements at each step (V_1, V_2, V_3), where V_1, V_2, V_3 represent the voltages at the clockwise rotation, counter-clockwise rotation, and original location $(\psi = 0)$, respectively.

5. The new turning angle ϕ_p of the rotating base is calculated by taking a weighted average of these signals at three steps:

$$\phi_p = \frac{\psi V_1 - \psi V_2}{V_1 + V_2 + V_3} \tag{4.1}$$

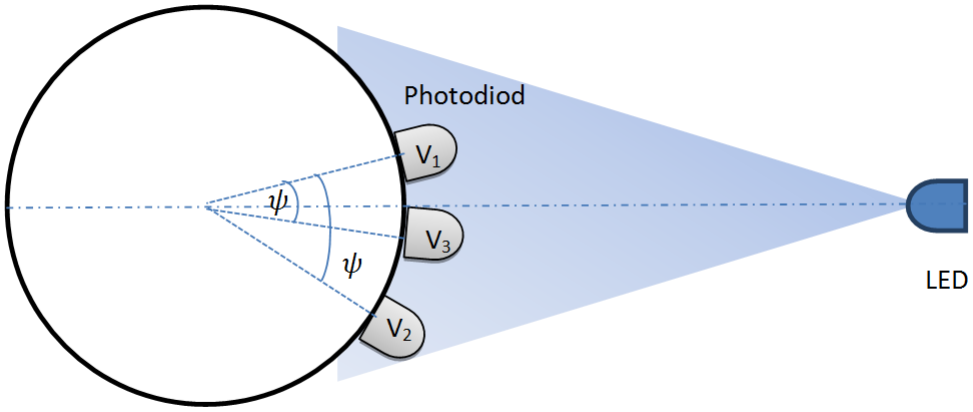

Figure 4.1 Illustration of the active alignment control algorithm.

4.2 Experimental Results

A mobile robot is used to confirm the feasibility of the algorithm. To set up the experiment (see Figure 4.2), the transmitter is fixed in a position while the receiver with the rotating base is mounted on a mobile robot (3WD 48mm Omni Wheel Arduino Mobile Robot Kit

from NEXUS robot), which is programmed to rotate (-60,60) degrees around its center axis continuously. The probing angular rotation for the rotating is $\psi = 5\ ^{\circ}$. The purpose of the experiments is to measure the rotating base rotation angle and the received signal strength when the control is on and off at three different distances (1 m, 2 m, 3 m). Figures 4.3, 4.5, and 4.7 show that the rotating base is able to counteract the rotational movement of the robot, to keep the receiver aligned approximately with the light coming from the transmitter, for all three distances tested. Figures 4.4, 4.6, 4.8 show the voltage signals received at the receiver in two cases, when the algorithm is enabled and disabled, respectively. It can be seen that, when the algorithm is turned on, the signal strength is above the threshold value of 1 V for most of the time; on the other hand, the signal strength is lower than the threshold value for much of the duration when the algorithm is turned off, and the situation worsens as the distance of communication increases. Finally, a data-transmitting test is conducted, where the baud rate is 115200 kbps and the amount of data sent is 83500 bytes. During these experiments the BER (bit error rate) is found to be zero for all conditions, but some data are lost due to the movement of the robot. Table 4.1 compare the amount of data lost when the active alignment control is turned on and off, respectively. The advantage of the proposed alignment control scheme is evident.

Table 4.1 Data lost due to robot movement.

Distance (m)	Data lost (control on)	Data lost (control off)
1	3132 bytes	9392 bytes
2	5218 bytes	31312 bytes
3	8300 bytes	46968 bytes

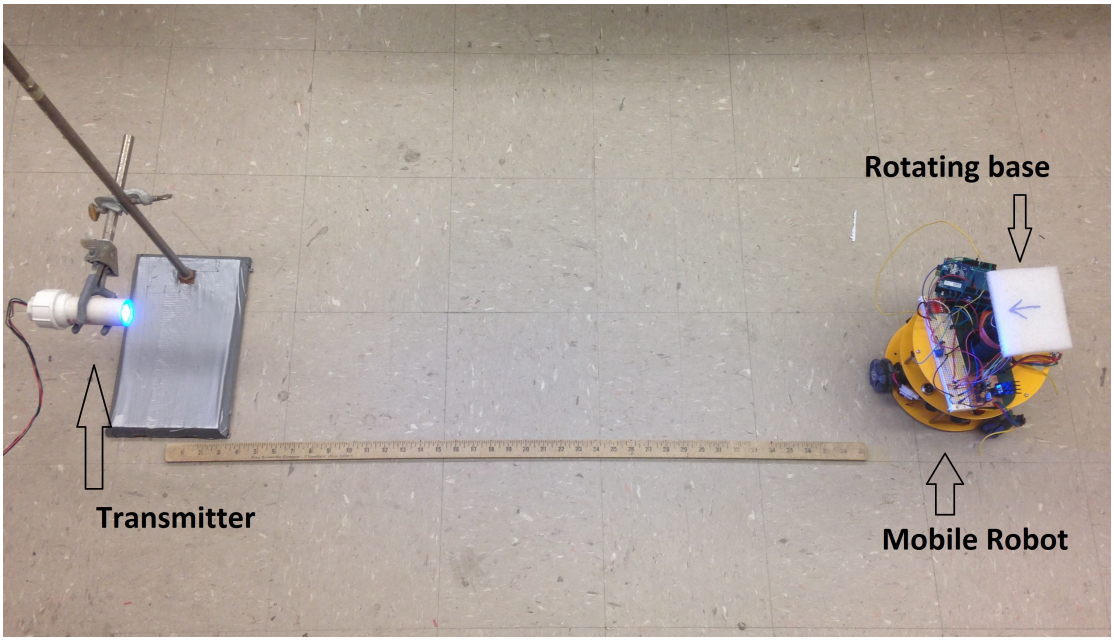

Figure 4.2 Experimental setup for testing the active alignment control algorithm.

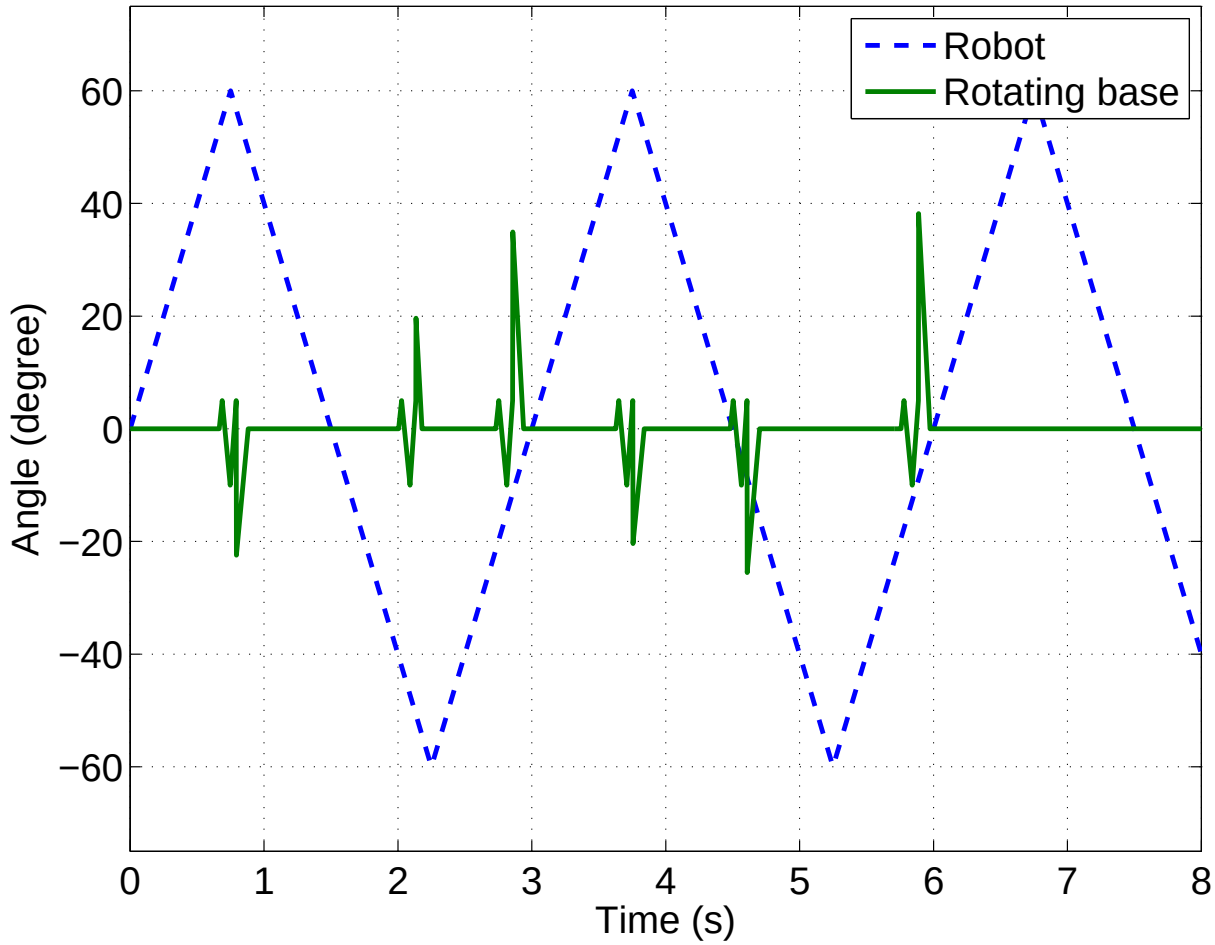

Figure 4.3 Measured rotation angle for the receiver base in response to the rotation angle of the robot platform, when the receiver is at 1 meter distance from the transmitter.

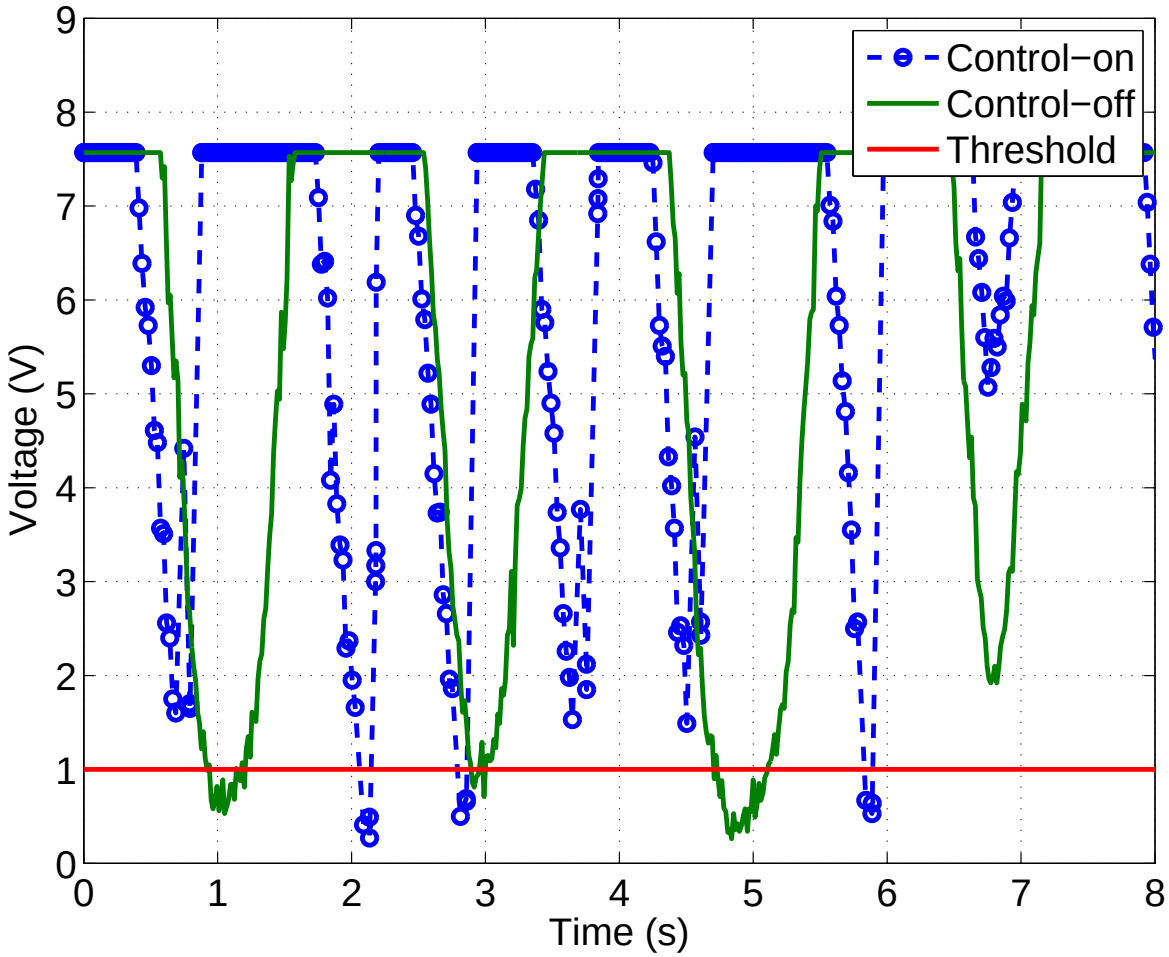

Figure 4.4 Measured signal strengths when the alignment control is on and off, respectively, when the receiver is at a distance of 1 m from the transmitter.

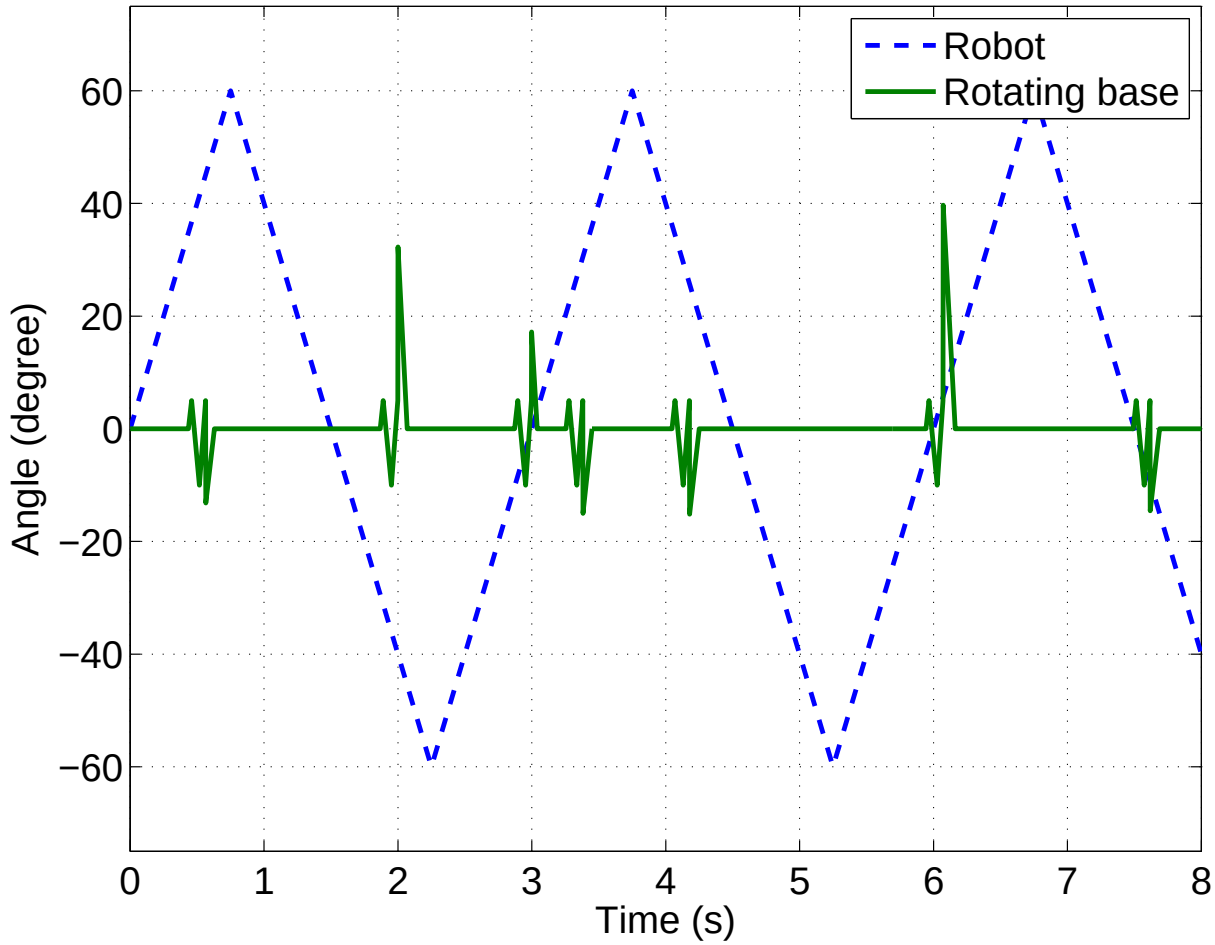

Figure 4.5 Measured rotation angle for the receiver base in response to the rotation angle of the robot platform, when the receiver is at 2 meter distance from the transmitter.

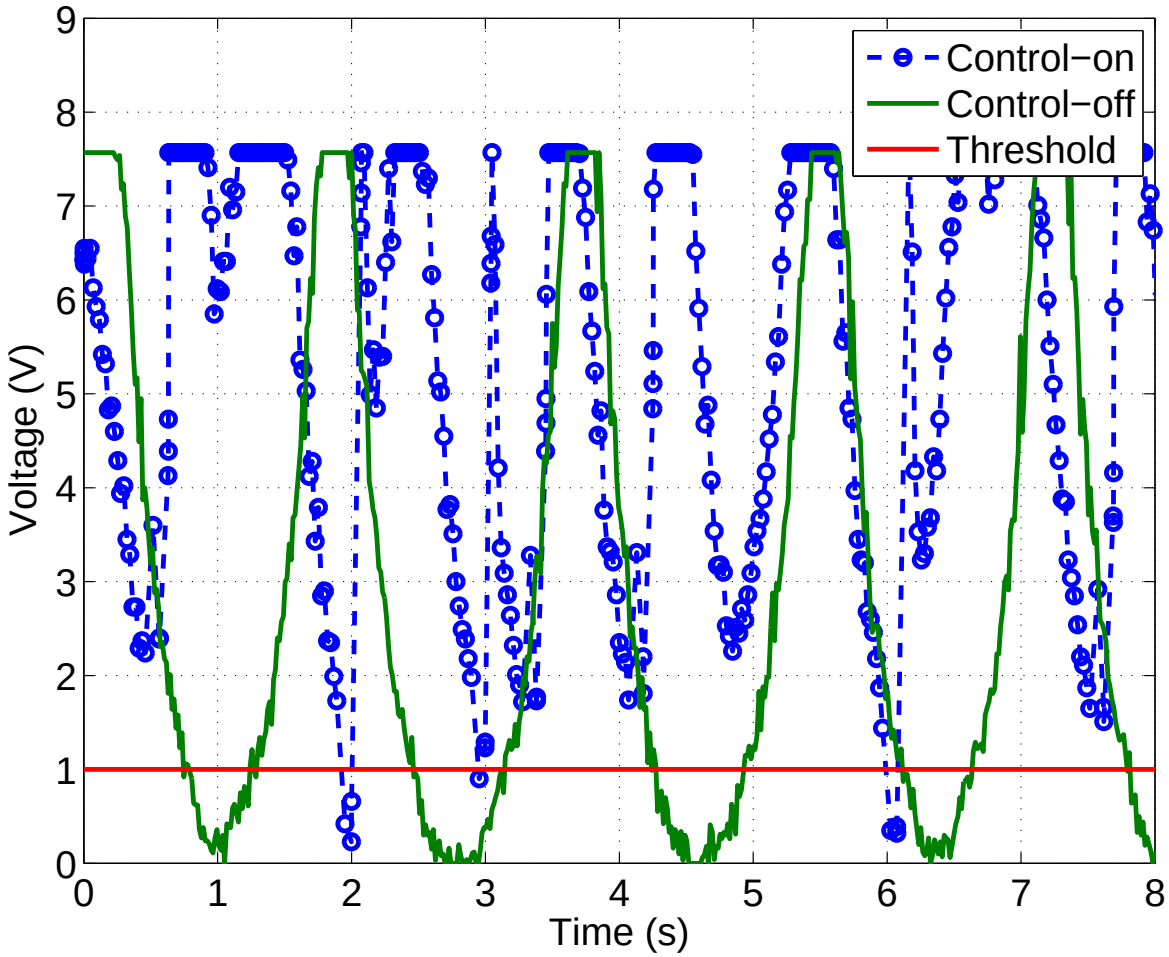

Figure 4.6 Measured signal strengths when the alignment control is on and off, respectively, when the receiver is at a distance of 2 m from the transmitter.

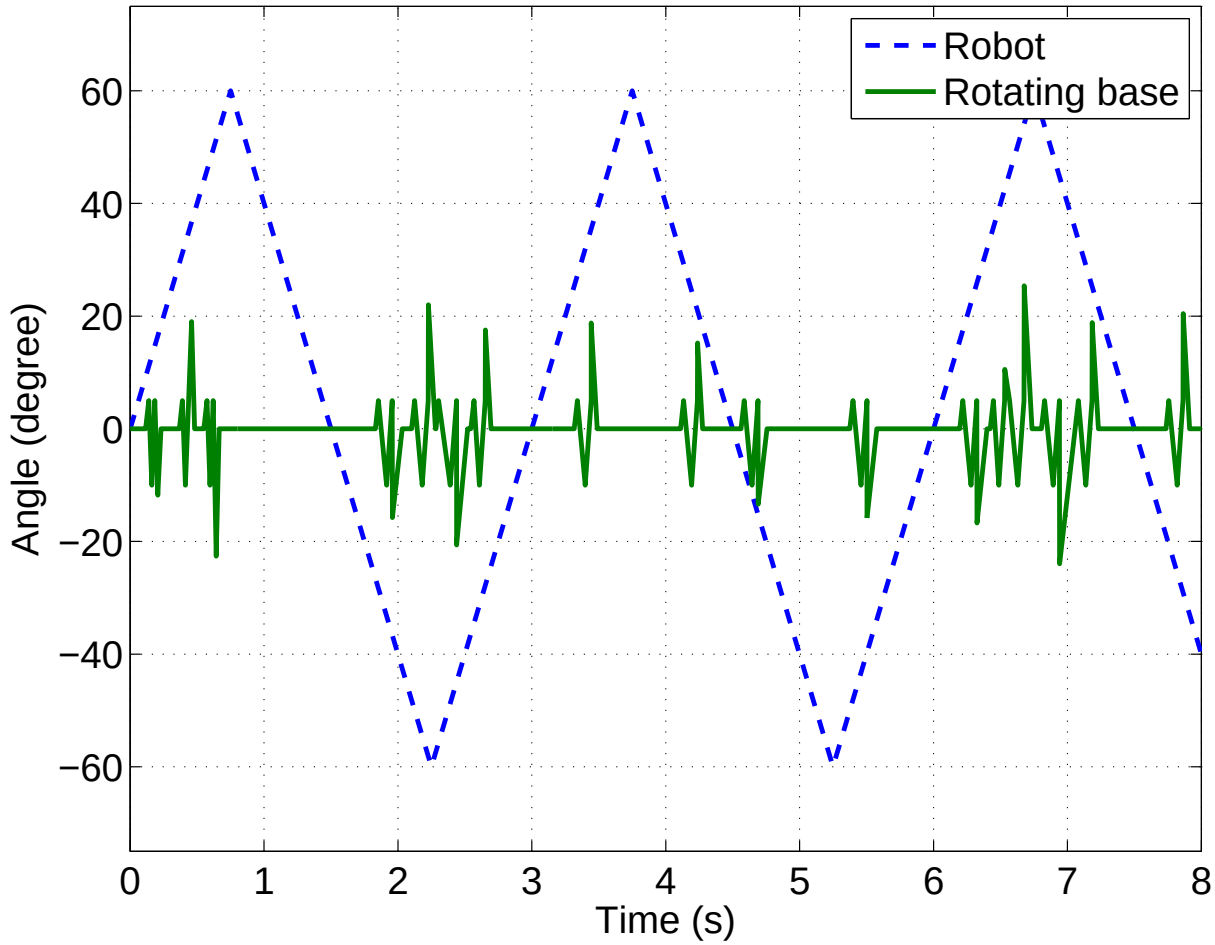

Figure 4.7 Measured rotation angle for the receiver base in response to the rotation angle of the robot platform, when the receiver is at 3 meter distance from the transmitter.

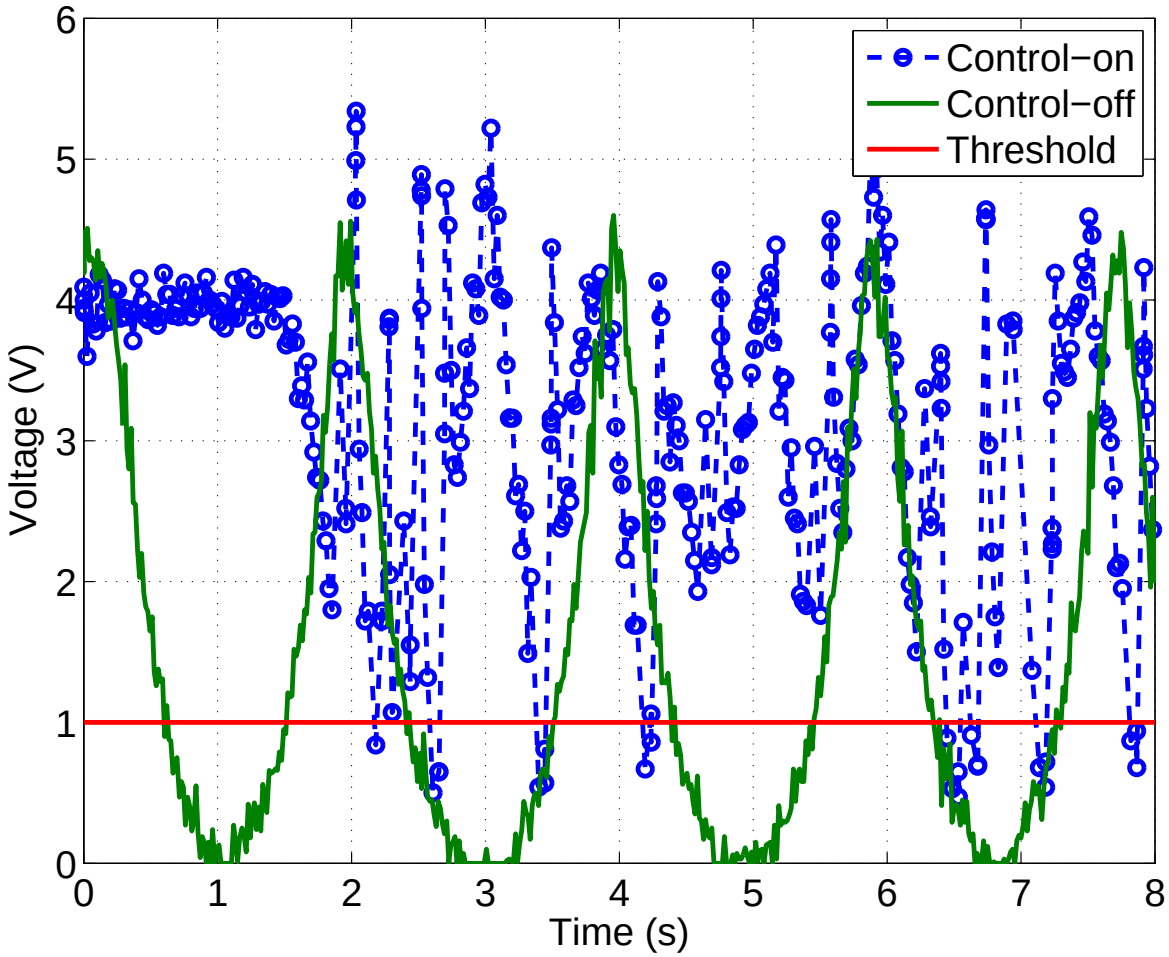

Figure 4.8 Measured signal strengths when the alignment control is on and off, respectively, when the receiver is at a distance of 3 m from the transmitter.

Chapter 5

Conclusion and Future Work

5.1 Conclusion

In this thesis a wireless optical communication system has been built using blue light. This device is able to send data with a rate up to 115200 kbps at distances of up to 23 m in an underwater setting, showing its promise in underwater mobile sensing and navigation applications.

A model for estimating the optical signal strength has been developed and validated through a series of experiments in air. This model allows for predictions to be made about the expected signal strength, which can be used to estimate the link quality and to estimate the relative distance and pose between the transmitter and the receiver. The latter will be instrumental in the design of active alignment control algorithms. Due to constraints on experimental conditions, the model has only be validated in air. However, we expect it to be valid for the underwater environment, but with different system parameters.

An active control algorithm has been presented for maintaining the alignment of the receiver with the transmitter for LED-based communication systems. The algorithm uses the received signal strength as feedback for adjusting the receiver angles. A mobile robot has been used to validate this algorithm.

5.2 Future Work

The systems and algorithms presented in this thesis lay the groundwork for pursuing further research on the refinement and application of LED-based optical communication systems, especially for the underwater setting. An immediate extension will be to explore the performance of the active alignment control algorithm underwater, where the transceivers are mounted on two underwater robots.

On the algorithm side, it will be of interest to use extended Kalman filters to estimate the relative distance and pose between the transmitter and the receiver, both of which could be on mobile robots, and to develop more advanced alignment control schemes.

While the wireless optical system creates the necessary backbone for low-latency and high-rate rate links , the current design is prone to feedthrough interference; namely, the receiver receives a spurious signal when the transmitter on the receiver side is transmitting. Therefore, the current system does not allow duplex-mode communication. Improvement of the system design to alleviate this problem is another direction of future work. In particular, extending communications into full duplex mode.

Finally, the current rotating base can only respond about a single axis. Consequently, it requires two communicating robots to stay in the same plane. This limitation can be overcome if an active pan-tilt base for the transmitter/receiver circuits is adopted. This idea and the corresponding alignment control problem represent another direction worthy of exploration.

BIBLIOGRAPHY

BIBLIOGRAPHY

[1] S. Climent, A. Sanchez, J. V. Capella, N. Meratnia, and J. J. Serrano, "Underwater acoustic wireless sensor networks: Advances and future trends in physical, mac and routing layers," *Sensors*, vol. 14, no. 1, p. 795, 2014. [Online]. Available: http://www.mdpi.com/1424-8220/14/1/795

[2] H. Brundage., "Designing a wireless underwater optical communication system," Master's thesis, Massachusetts Institute of Technology, 2010.

[3] S. N. White, A. D. Chave, and G. T. Reynolds, "Investigations of ambient light emission at deep-sea hydrothermal vents," *Journal of Geophysical Research: Solid Earth*, vol. 107, no. B1, pp. EPM 1–1–EPM 1–13, 2002. [Online]. Available: http://dx.doi.org/10.1029/2000JB000015

[4] Wikipedia, "Light-emitting diode," March 2012, https://en.wikipedia.org/wiki/Light-emitting-diode.

[5] ——, "Laser diode," June 2015, https://en.wikipedia.org/wiki/Laser-diode.

[6] Superbrightleds, "Cree-xre-series-1-watt-blue-led," March 2014, https://www.superbrightleds.com/moreinfo/high-powered/cree-xre-series-1-watt-blue-led-b4k/933/1875/.

[7] CREE, "Cree xlamp xr-e led," January 2006, http://www.cree.com/ /media/files/cree/led20components20and20modules/xlamp/xlamp7090xre.pdf.

[8] Electrotechservices, "Mosfet types," February 2015, http://www.electrotechservices.com/electronics/metaloxidesemiconductorfets.

[9] Wikipedia, "Photoresistor," March 2015, https://en.wikipedia.org/wiki/Photoresistor.

[10] ——, "Phototransistor," March 2015, https://wikimedia.org/wiki/phototransistor.jpg.

[11] ——, "Photodiode," March 2015, https://en.wikipedia.org/wiki/Photodiode.

[12] ——, "Avalanche photodiode," March 2015, https://en.wikipedia.org/wiki/Avalanche-photodiode.

[13] ——, "Photomultiplier," March 2015, https://en.wikipedia.org/wiki/Photomultiplier.

[14] S. B. Alexander, *Optical Communication Receiver Design*. SPIE, 1997.

[15] NOAA, "Ocean," August 2012, http://www.noaa.gov/ocean.html.

[16] WHOI, "Commonwealth awards $5 m R&D grant for center for marine robotics," Februray 2014, http://www.whoi.edu/news-release/center-for-marine-robotics.

[17] J. Catipovic, "Performance limitations in underwater acoustic telemetry," *Oceanic Engineering, IEEE Journal of*, vol. 15, no. 3, pp. 205–216, Jul 1990.

[18] SounLink, "Underwater acoustic modem," April 2006, http://www.link-quest.com/html/intro1.htm.

[19] P. P. Smyth, P. L. Eardley, K. T. Dalton, D. R. Wisely, P. McKee, and D. Wood, "Optical wireless: a prognosis," vol. 2601, 1995, pp. 212–225. [Online]. Available: http://dx.doi.org/10.1117/12.228143

[20] M. Chen, S. Zhou, and T. Li, "The implementation of ppm in underwater laser communication system," in *Communications, Circuits and Systems Proceedings, 2006 International Conference on*, vol. 3, June 2006, pp. 1901–1903.

[21] W. Cox, "1 mbps underwater communication system using a 405nm laser diode and photomultiplier tube," Master's thesis, North Carolina State University, 2008.

[22] F. Hanson and S. Radic, "High bandwidth underwater optical communication," *Appl. Opt.*, vol. 47, no. 2, pp. 277–283, Jan 2008. [Online]. Available: http://ao.osa.org/abstract.cfm?URI=ao-47-2-277

[23] R. Hagem, D. V. Thiel, S. O'Keefe, A. Wixted, and T. Fickenscher, "Low-cost short -range wireless optical fsk modem for swimmers feedback," in *Sensors, 2011 IEEE*, Oct 2011, pp. 258–261.

[24] F. Lu, S. Lee, J. Mounzer, and C. Schurgers, "Low-cost medium-range optical underwater modem: Short paper," in *Proceedings of the Fourth ACM International Workshop on UnderWater Networks*, ser. WUWNet '09. New York, NY, USA: ACM, 2009, pp. 11:1–11:4. [Online]. Available: http://doi.acm.org/10.1145/1654130.1654141

[25] F. Schill, U. R. Zimmer, and J. Trumpf, "Visible spectrum optical communication and distance sensing for underwater applications," in *In: Proc. of Australasian Conference on Robotics and Automation*, 2004.

[26] M. Doniec and D. Rus, "Bidirectional optical communication with AquaOptical II," in *Communication Systems (ICCS), 2010 IEEE International Conference on*, Nov 2010, pp. 390–394.

[27] D. Anguita, D. Brizzolara, and G. Parodi, "Building an underwater wireless sensor network based on optical: Communication: Research challenges and current results," in *Sensor Technologies and Applications, 2009. SENSORCOMM'09. Third International Conference on*. IEEE, 2009, pp. 476–479.

[28] ——, "Optical wireless communication for underwater wireless sensor networks: Hardware modules and circuits design and implementation," in *OCEANS 2010*. IEEE, 2010, pp. 1–8.

[29] I. Rust and H. Asada, "A dual-use visible light approach to integrated communication and localization of underwater robots with application to non-destructive nuclear reactor inspection," *Robotics and Automation (ICRA), 2012 IEEE International Conference on*, pp. 2445–2450, May 2012.

[30] S. Hranilovic, *Wireless Optical Communication Systems*. New York, NY, USA: Springer-Verlag New York, Inc., 2009.

[31] E. F. Schubert, T. Gessmann, and J. K. Kim, *Light Emitting Diodes*. John Wiley Sons, Inc., 2000. [Online]. Available: http://dx.doi.org/10.1002/0471238961.1209070811091908.a01.pub2

[32] J. M. Kahn and J. R. Barry, "Wireless infrared communications," *Proceedings of the IEEE*, vol. 85, no. 2, pp. 265–298, 1997.

[33] L. A. Coldren, S. W. Corzine, and M. L. Mashanovitch, *Diode lasers and photonic integrated circuits*. John Wiley & Sons, 2012, vol. 218.

[34] G. Keiser, *Optical fiber communications*, ser. McGraw-Hill series in electrical and computer engineering: Communications and signal processing. McGraw-Hill, 2000. [Online]. Available: http://books.google.com/books?id=lANTAAAAMAAJ

[35] L. Yuan, S. Liu, M. Chen, and X. Luo, "Thermal analysis of high power led array packaging with microchannel cooler," in *Electronic Packaging Technology, 2006. ICEPT '06. 7th International Conference on*, Aug 2006, pp. 1–5.

[36] LUXDRIVE, "3021/3023 buckpuck," January 2007, http://www.digikey.com/catalog/en/partgroup/buckpuck30213023series/28982.

[37] P. Scherz, *Practical Electronics for Inventors*, 2nd ed. New York, NY, USA: McGraw-Hill, Inc., 2007.

[38] I. Rectifire, "Irf7307pbf," January 2013, http://www.digikey.com/IRF7307PBFCT-ND/812597.

[39] N. V. Tkachenko, *Optical spectroscopy: methods and instrumentations*. Elsevier, 2006.

[40] T. Instruments, "High voltage high slew rate wideband fet-input operation amplifire," March 2006, http://www.ti.com/product/ths4631.

[41] MOFLON, "Mt007 slip ring," January 2008, http://www.moflon.com/mt007.html.

[42] J. Jiang, S. To, W. Lee, and B. Cheung, "Optical design of a freeform tir lens for led streetlight," *Optik International Journal for Light and Electron Optics*, vol. 121, no. 19, pp. 1761 – 1765, 2010. [Online]. Available: http://www.sciencedirect.com/science/article/pii/S0030402609002083

[43] M. Doniec, M. Angermann, and D. Rus, "An end-to-end signal strength model for underwater optical communications," *Oceanic Engineering, IEEE Journal of*, vol. 38, no. 4, pp. 743–757, Oct 2013.

[44] F. Miller, A. Vandome, and J. McBrewster, *Beer-Lambert Law*. VDM Publishing, 2009. [Online]. Available: https://books.google.com/books?id=XO-DQgAACAAJ